Probing QCD in the nuclear medium with real photons and nuclear targets at GlueX

M. Dugger, B. G. Ritchie, N. Sparks
Arizona State University, Tempe, Arizona 85287, USA

E. G. Anassontzis, C. Kourkoumeli, G. Vasileiadis
National and Kapodistrian University of Athens, 15771 Athens, Greece

N. S. Jarvis, W. I. Levine, M. McCracken, W. McGinley, C. A. Meyer, R. A. Schumacher, M. J. Staib
Carnegie Mellon University, Pittsburgh, Pennsylvania 15213, USA

G. Kalicy, D. I. Sober
Catholic University of America, Washington, D.C. 20064, USA

A. Barnes, R. T. Jones, J. McIntyre, F. Mokaya, B. Pratt
University of Connecticut, Storrs, Connecticut 06269, USA

H. Gao (Spokesperson), C. Gu, X. Li, T. Liu, C. Peng, W. Xiong, X. Yan, Z. Zhao
Duke University, Durham, North Carolina 27708, USA

W. Boeglin, L. Guo, M. Kamel, W. Phelps, J. Reinhold
Florida International University, Miami, Florida 33199, USA

H. Al Ghoul, B. E. Cannon, V. Crede, A. Ernst, P. Eugenio, A. I. Ostrovidov, A. Tsaris
Florida State University, Tallahassee, Florida 32306, USA

W. J. Briscoe, F. J. Klein, I. I. Strakovsky
The George Washington University, Washington, D.C. 20052, USA

D. G. Ireland, K. Livingston, P. Pauli, D. Werthmüller
University of Glasgow, Glasgow G12 8QQ, United Kingdom

A. Ali, R. Dzhygadlo, K. Goetzen, A. Hamdi, F. Nerling, K. J. Peters, C. Schwarz, J. Schwiening
GSI Helmholtzzentrum für Schwerionenforschung GmbH, D-64291 Darmstadt, Germany

J. Frye, R. E. Mitchell, M. R. Shepherd, A. Subedi, J. Zarling
Indiana University, Bloomington, Indiana 47405, USA

A. Dolgolenko, V. S. Goryachev, I. Larin, V. Matveev, V. Tarasov
Institute for Theoretical and Experimental Physics, Moscow 117259, Russia

A. Austregesilo, F. Barbosa, T. Britton, E. Chudakov, M. M. Dalton, A. Deur, H. Egiyan, S. Furletov, D.W. Higinbotham, M. M. Ito, D. Lawrence, D. Mack, P. T. Mattione, M. McCaughan, L. Pentchev, E. Pooser, E. S. Smith, A. Somov (Spokesperson), S. Taylor, T. Whitlatch, B. Zihlmann
Thomas Jefferson National Accelerator Facility,
Newport News, Virginia 23606, USA

R. Miskimen
University of Massachusetts, Amherst, Massachusetts 01003, USA

R. Cruz-Torres, C. Fanelli, S. Gilad, J. Hardin, O. Hen*,
G. Laskaris, A. Papadopoulou, M. Patsyuk (Spokesperson),
A. Schmidt, B.A. Schmookler, E.P. Segarra, M. Williams, Y. Yang
Massachusetts Institute of Technology, Cambridge, Massachusetts 02139, USA

K. Assumin-Gyimah, H. Bhatt, D. Bhetuwal, D. Dutta (Spokesperson),
J. Dunne, L. El-Fassi, L. Kabir, A. Karki, L. Ye
Mississippi State University, Mississippi State, Mississippi 29762, USA

V. V. Berdnikov, D. Romanov, S. Somov
National Research Nuclear University
Moscow Engineering Physics Institute, Moscow 115409, Russia

C. Salgado
Norfolk State University, Norfolk, Virginia 23504, USA

A. Gasparian, M. Levillain, R. Pedroni
North Carolina A&T State University, Greensboro, North Carolina 27411, USA

T. Black, L. Gan
University of North Carolina at Wilmington,
Wilmington, North Carolina 28403, USA

S. Dobbs, L. Robison, K. K. Seth, A. Tomaradze, T. Xiao
Northwestern University, Evanston, Illinois 60208, USA

L.B. Weinstein (Spokesperson), F. Hauenstein
Old Dominion University, Norfolk, Virginia 23529, USA

T. D. Beattie, A. M. Foda, G. M. Huber, G. J. Lolos, Z. Papandreou,
A. Yu. Semenov, I. A. Semenova, A. Teymurazyan
University of Regina, Regina, Saskatchewan, Canada S4S 0A2

A. Ashkenazi, E. Cohen, M. Duer, J. Lichtenstadt,
E. Piasetzky (Spokesperson), O. Reich
Tel-Aviv University, Tel Aviv 69978, Israel

A. Beck, I. Korover, and S. Maytal-Beck
Nuclear Research Center Negev, Beer-Sheva 84190, Israel

W. Brooks, H. Hakobyan, S. Kuleshov, O. Soto, J. Vega
Universidad Técnica Federico Santa María, Casilla 110-V Valparaíso, Chile

V. Gauzshtein, I. Kuznetsov, V. Lyubovitskij
Tomsk State University, 634050 Tomsk, Russia
Tomsk Polytechnic University, 634050 Tomsk, Russia

N. Gevorgyan, V. Kakoyan, H. Marukyan
A. I. Alikhanian National Science Laboratory
(Yerevan Physics Institute), 0036 Yerevan, Armenia

J. R. Stevens
College of William and Mary, Williamsburg, Virginia 23185, USA

S. Han, N. Qin, Z. Zhang, X. Zhou
Wuhan University, Wuhan, Hubei 430072, People's Republic of China

Theory Support

M. Strikman	Pennsylvania State University, State College, PA.
G.A. Miller	University of Washington, Seattle, WA.
A.B. Larionov	Frankfurt Institute for Advanced Studies (FIAS), and National Research Centre "Kurchatov Institute", Moscow, Russia.
M. Sargsian	Florida International University, Miami, FL.
L. Frankfurt	Tel-Aviv University, Tel Aviv, Israel.

Abstract

Photonuclear reactions using real photons offer a unique probe for fundamental aspects of QCD in the nuclear medium, as well as a stringent test for the interpretation of electro-induced hard knockout reactions off nuclei. We propose to measure the $A(\gamma, X)$ and $A(\gamma, XN_{\rm recoil})$ reactions (here, X represents a wide range of baryon-meson final states) over a wide range of momentum transfers for $A = {}^{2}$H, ^{4}He, and ^{12}C and ^{40}Ca nuclei. The experiment is proposed to take place in Hall D using the GlueX spectrometer in its standard configuration and the standard Hall D tagged coherent bremsstrahlung photon beam. The data will be used to address the following issues:

- Structure of the photon as observed via the transition between hadronic (vector-meson) to partonic (point-like) couplings,
- Color transparency in large momentum transfer reactions,
- Reaction mechanism sensitivity of short-range correlations in nuclei.

We estimate this measurement will require a total of 40 days at an electron beam energy of 12 GeV.

*Contact Person: hen@mit.edu

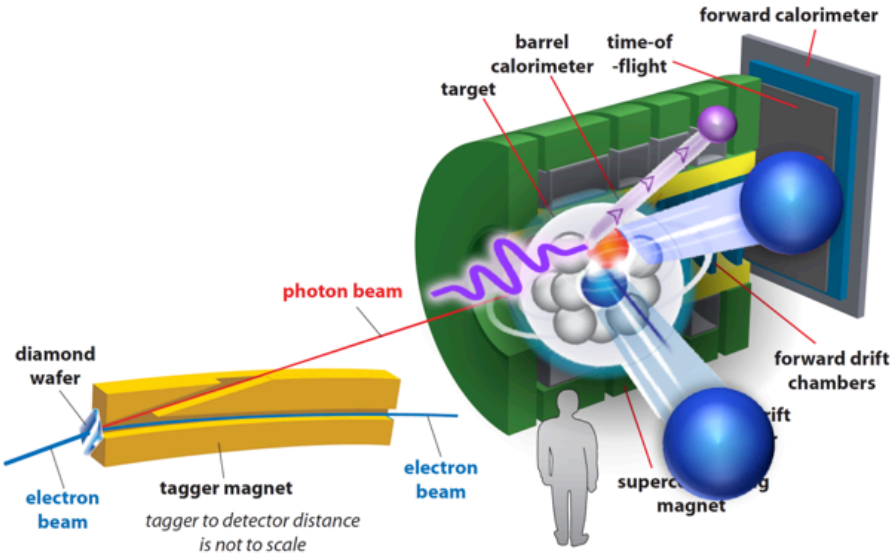

1 Scientific Motivation

Exclusive photonuclear reactions on atomic nuclei offer a unique probe to study various aspects of QCD in the nuclear medium. These include, among others, the structure of the photon, point-like configurations (PLCs) of nucleons, and color transparency (CT). Photonuclear reactions can also provide valuable information on specific aspects of nuclear structure in a way that is complementary to electro-induced quasi-elastic knockout reactions. In this section, we list the scientific motivations for the different physics aspects of the proposed experiment.

Considering the QCD description of atomic nuclei, understanding the interplay between partonic and nucleonic degrees of freedom has been a long-standing goal of modern nuclear physics research in general, and of the Jefferson Lab physics program in particular [1]. Active areas of study that combine nucleonic and partonic effects include searches for color transparency [2], studies of the European Muon Collaboration (EMC) effect [3–6], and studies of short-range correlations (SRCs) in nuclei [5–8]. Recent theoretical studies consistently link the three (CT, EMC and SRC) as being due to the effect of the nuclear medium on point-like configurations in the bound nucleon wave function. In these models, the EMC effect is explained as a result of the suppression of PLCs in the bound nucleon wave function, which is emphasized when the bound nucleon is highly-virtual (i.e., far off its mass-shell). Such high-virtuality nucleonic states are expected to be dominated by SRCs, while PLCs are the leading candidate to induce color transparency effects at large momentum transfers. Therefore, the PLC-inspired models of the EMC effect, SRCs and CT are all intimately related and should be viewed together in a self-consistent description of QCD effects in nuclei. See Ref. [6] for recent review.

The phenomenology that links these effects together to a global picture of QCD in the nuclear medium relies heavily on experimental data that is either sparse (as in the case of hadron color transparency) or subject to interpretation uncertainties (as in the case of high-virtuality nucleons and SRCs). The proposed experiment seeks to measure a series of observables that will help clarify the connection between these effects, building toward a comprehensive global picture of high-energy QCD effects in nuclei.

Table 1: List of possible exclusive photonuclear reactions off protons and neutrons that are within the detection capabilities of the GlueX spectrometer. Note that neutron reactions are only possible using nuclear targets (deuteron and heavier).

Proton Reactions	**Neutron Reactions**
$\gamma + p \to \pi^0 + p$	$\gamma + n \to \pi^- + p$
$\gamma + p \to \pi^- + \Delta^{++}$	$\gamma + n \to \pi^- + \Delta^+$
$\gamma + p \to \rho^0 + p$	$\gamma + n \to \rho^- + p$
$\gamma + p \to K^+ + \Lambda^0$	$\gamma + n \to K^- + \Lambda^0$
$\gamma + p \to K^+ + \Sigma^0$	$\gamma + n \to K^0 + \Sigma^0$
$\gamma + p \to \omega + p$	—
$\gamma + p \to \varphi + p$	—

1.1 Photon Structure

Many detailed aspects of the nature of the photonuclear interaction are still largely unknown. At low momentum transfers, the photon is usually treated as superposition of hadronic (vector-meson) states of moderate masses, while, at higher momentum transfers, it is treated as a point-like particle due to a $1/t$ suppression of the vector-meson states. The transition between the two regimes is expected to occur at relatively moderate values of momentum transfer of a few GeV^2, but has never been mapped. The experimental discovery of this transition will help clarify the different interaction mechanisms of photonuclear reactions, the origin of constituent quark counting rules, and more.

As explained below, these questions can be addressed experimentally, using the GlueX spectrometer to measure exclusive photonuclear production processes off nuclei of the kind:

$$\gamma + A \to M + B + (A-1)^*$$

where M and B are an outgoing meson-baryon pair. See Tab. 1 for a list of reactions within the reach of the GlueX detection capabilities.

Nuclei provide a highly sensitive probe for the transition between soft (vector-meson) and hard (point-like) regimes of the photon interaction. A point-like photon does not interact strongly, and can penetrate the nucleus. The effective coherence length is essentially infinite and, therefore, the photon can interact with all nucleons, including those near the far surface of the nucleus. The interaction produces a pair of hadrons that, in order to be detected, must escape the nucleus without absorption. The measured cross section will depend on the overlap between the possible interaction regions with the regions of successful hadron escape, leading to specific dependence on the nuclear size, and thus A (Fig. 1).

In contrast, when the photon is in a hadronic state, it can only interact with nucleons on the rim of the nucleus (i.e., its coherence length and penetration capability are much smaller). In this case, the A dependence of the experimental cross section will be different, and the Glauber approximation can describe the process. Fig. 1 shows an illustration of the regions in the nucleus probed in the different photon interaction regime. Fig. 2 shows transparency calculations (ratio of experimental to plane-wave cross sections, referred to also in this report as reduced cross sections) for ^{4}He, ^{12}C and ^{40}Ca for the different photon interaction scenarios for the elementary reaction $\gamma n \to \pi^- p$ [9]. Fig. 3 shows the transparency calculations relative to ^{4}He, in order to highlight the A-dependence of the two regimes. As can be seen, the difference between the photon interaction mechanisms is very significant and can be observed in both the absolute value of the measured cross section and in its A-dependence. We note that the elementary cross section will be tested experimentally by measurements on hydrogen and deuterium targets.

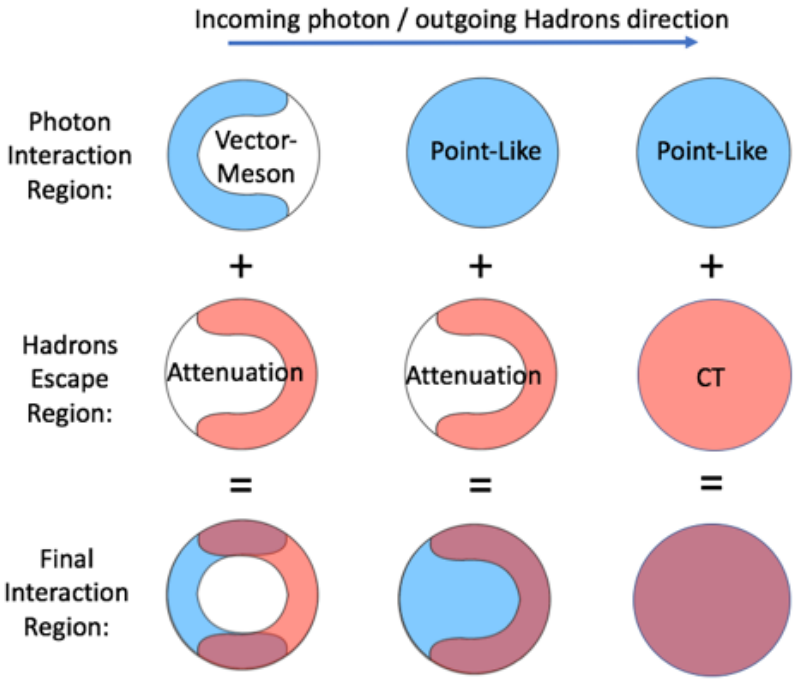

Figure 1: Illustration of the region in the nucleus probed in exclusive photonuclear production reactions under different photon interaction and hadron propagation assumptions. The blue shaded area shows the photon penetration region. The bright orange shaded area shows region from which the final state hadrons can escape without absorption and/or significant re-scattering. The red area shows the intersection of the two that defines the interaction region sampled by the experiment. As can be seen, in these idealized cases, the A-dependence of the nuclear cross section should scale between $A^{1/3}$ and A^1 for the interaction mechanisms relevant for GlueX kinematics (see Fig. 2 for full calculations).

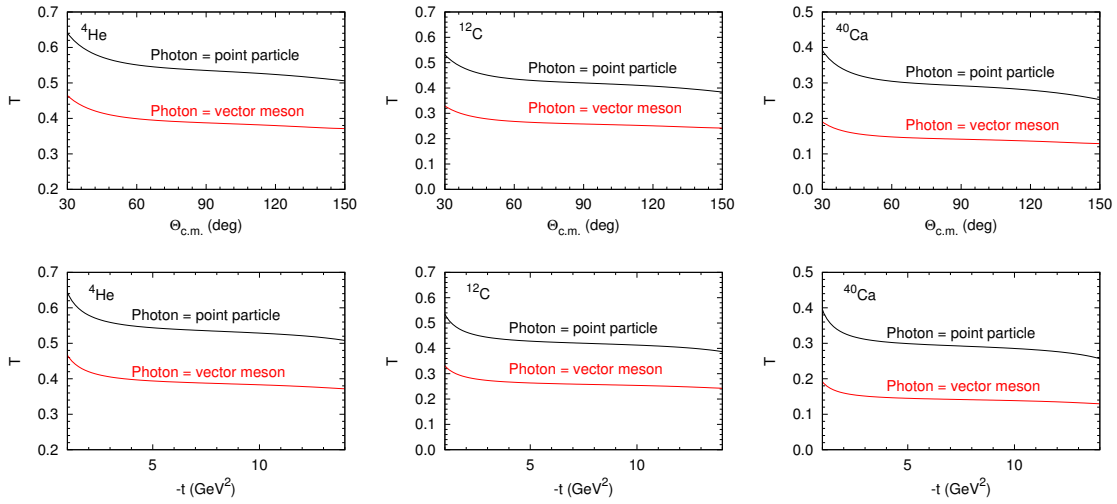

Figure 2: Calculated transparency (ratio of full calculation to plane wave calculation) for pion photoproduction reaction off a neutron ($\gamma n \to \pi^- p$) in ^{4}He (left column), ^{12}C (middle column), and ^{4}0Ca (right column) as a function of the center-of-mass scattering angle (top row) and momentum transfer t (bottom row). The different lines correspond to calculations describing the photon interaction as a superposition of vector mesons (red) and as a point-like particle (black), See Ref. [9] for details.

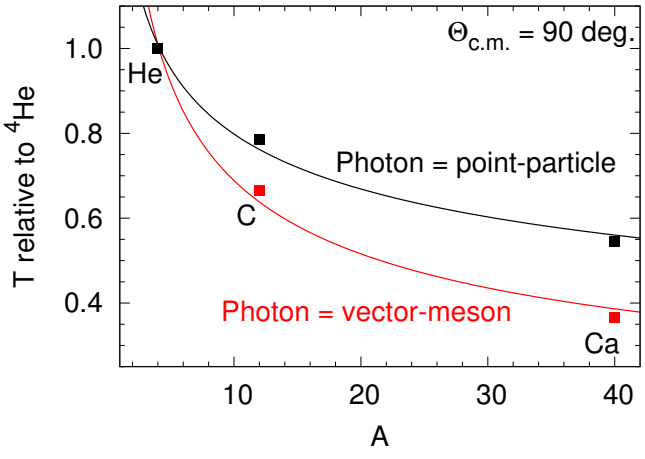

Figure 3: The calculated transparency for $\gamma n \to \pi^- p$ at $\theta_{cm} = 90°$, relative to that of ^{4}He, so as to highlight the A-dependence of the two regimes. The data points are calculations from Ref. [9] for ^{4}He, ^{12}C, and ^{40}Ca, while the curves are a simple power-law fit to the data points.

The Hall D beam line and the GlueX detector allow the study of a large number of hard exclusive reaction channels characterized by a large variety of emerging particles in the final state (η, φ, K^+, K^{+*}, $\Lambda \ldots$), as seen in table 1. Assuming the transition between vector meson and point-like photon regimes to occur at about $|t| = 2$ GeV^2 [9], we can map the transition experimentally for multiple channels. This is a large advantage of the GlueX spectrometer, as the transition might depend on the quark composition (accessible by comparing π and η) and/or the spin of the final state (accessible by comparing π and ρ).

1.2 Color Transparency

At high momentum transfers, it is also expected that the point-like photon will preferably couple to point-like configurations in the nucleon wave-function [2, 6]. Due to the smaller size of these configurations, their effective color dipole (or tripole) moment should be significantly smaller. This is expected to lead to a reduced interaction as the nucleon propagates through the surrounding nuclear environment. This phenomenon is commonly referred to as color transparency (CT).

As CT is a distinctive prediction of QCD, its study has a long history in the search for signatures of QCD in nuclei. CT is essential for Bjorken scaling in deep inelastic scattering (DIS) at high energies [8], thus the observation of scaling in DIS can be considered as evidence for CT at high energies, i.e., in the perturbative QCD regime. At intermediate energies, CT provides a unique probe of the space-time evolution of wave packets, and, therefore, the onset of CT may be identified with the onset of QCD in nuclei. Thus far experimentally, the onset of CT has been only been observed for mesons [10, 11], but not for baryons [12, 13].

The concept of CT arises from the idea that scattering processes at sufficiently high momentum transfer preferentially select amplitudes in the initial and final state hadrons that are characterized by a small transverse size (i.e. PLCs). The dominance of these small-size configurations in exclusive hard reactions is also referred to as squeezing [14]. The PLC should be 'color neutral' outside of its small radius in order that it not radiate gluons, resulting in color screening. If the compact size is maintained for distances comparable to the size of the nucleus, i.e., if the size of the PLC stays frozen, then it would pass through the nuclear medium without further interactions with the medium. The freezing of the expansion scale of the small configuration is governed by the energy transfer of the hard reaction. This implies that nuclear transparency (defined as the ratio of the cross section per nucleon for an exclusive scattering process on a bound nucleon in the nucleus to the cross section for the same process on a free nucleon) is an ideal observable to search for the onset of CT.

Both squeezing and freezing are required to observe CT. A small-sized configuration that expands significantly before exiting the nucleus will be attenuated similar to a 'regular'-sized configuration. Only the combination of the squeezing and freezing effects would lead to an increase in the measured nuclear transparency as a function of momentum transfer or energy. In the traditional nuclear physics picture (also known as Glauber approximation), the scattering process at high energies is described by small-angle scattering and a mean free path modulated by the free nucleon cross section [15]. The Glauber nuclear transparency is expected to be independent of energy and momentum transfer since the free nucleon cross section is also similarly independent at intermediate energies. Thus, a large rise in the nuclear transparency as a function of momentum or energy transfer is a clear signature for the onset of CT.

It should be mentioned that leading models of the EMC effect relate it to the suppression of PLCs in the bound nucleon wave function as they are expected to dominate the bound nucleon structure function at high-x [2, 6, 16, 17]. CT and the EMC effect are therefore intimately related, as they are in fact driven by the same physics. The observation of CT for hadrons in hard, large momentum transfer reactions will therefore prove the important (dominant) role played by PLCs in these reactions, thereby confirming their large contribution to the EMC effect.

High-energy and large-angle scattering processes are a natural tool for searching for CT effects.

The hard processes with large momentum transfers enhance squeezing by emphasizing the contribution of the minimal Fock state (PLC) with a reduced interaction, while freezing is expected to be dominated by the energy transfer of the reaction. In that sense, due to their large energy transfers, photonuclear reactions have an inherent advantage in searching for CT effects. Nevertheless, past searches for the onset of CT have been predominantly carried out via lepton- and hadron-induced hard exclusive processes and not photonuclear ones.

A unique feature of photonuclear reactions is that the entire energy of the photon is transferred in the reaction, regardless of the momentum transfer. At Hall-D photon energies, this helps ensure significant freezing of the expansion times even for moderate momentum transfers, thus sampling a completely different (and complementary) phase-space as compared to past and future $(e, e'p)$ measurements. The photon probe allows the interaction vertices to be uniformly distributed throughout the nuclear volume. However, without CT, the requirement to detect the emerging final state particles restricts the interaction vertex to the outer rim of the nucleus, the only region from which these particles can escape without considerable re-interaction. As illustrated in Fig. 1, the CT-induced reduction in the outgoing-hadron attenuation should increase the total cross section and bringing it's A-dependence closer to linear. For the kinematical phase-space accessible with the Hall D beam and GlueX spectrometer, Ref [9] predicts large CT effects that can be observed in the ratio of the measured cross section to Glauber calculations at large momentum transfers. Fig. 4 shows example calculations for GlueX kinematics [9]. As can be seen, large CT effects appear over a wide range of $|t|$ and center-of-mass (c.m.) frame scattering angles. Another feature of photonuclear reactions is the fact that the $|t|$ and $|u|$ dependences of the measured transparency (outside 90° scattering in the c.m. frame) can provide information on the individual CT effects on the propagation of the final state meson and baryon.

It is important to note that these measurements also allow for the determination of the effective cross section for the scattering of the outgoing particles off a nucleon ($\sigma_{\eta N}$, $\sigma_{\Phi N}$, ...). The constituent quark counting model describes well the ratio between the πN, KN, and NN cross sections [18–20], but not necessarily other meson-nucleon cross sections. Some of these can be extracted from the GlueX photoproduction data. This data will lead to a better understanding of processes that cannot be well described by simple perturbative quark counting. The sensitivity to the effective rescattering cross section is demonstrated in Fig. 5, where the transparency ratio between the reactions is shown for different effective cross sections. Comparing different exclusive photoproduction reactions in different nuclei over a wide range of kinematics, including those that are optimal for observing CT, will help improve our understanding of the underlying dynamics of these rescattering processes. Therefore, the study of the nuclear transparency of the different particles produced at the hard photon absorption vertex has scientific merit in its own right.

To summarize, under the proposed kinematical conditions, major deviations from the standard Glauber calculation and perturbative quark counting predictions are expected. These deviations are associated with the nature of the rescattering mechanism and the type of the rescattered particles. The simultaneous measurement of a few reaction channels and the ability to create ratios and super-ratios of transparencies will allow us to study these processes with small systematic and statistical uncertainties and to strongly constrain the theoretical interpretation. These measurements will complement the approved 12 GeV experiment to study CT in pion and ρ^- electroproduction, as well as in quasielastic proton knockout.

1.3 Nuclear Structure (SRC)

Short-range correlations (SRCs) refer to the pairing of nucleons in nuclei which are close together such that their wave functions overlap. In momentum space, these SRC pairs are characterized by having high relative momentum and low center of mass momentum, where high and low are relative to the Fermi-momentum (k_F) of the nucleus. See Refs [5–7] for recent reviews.

The short-range structure of nuclei is an active and vibrant field of research. Recent works have

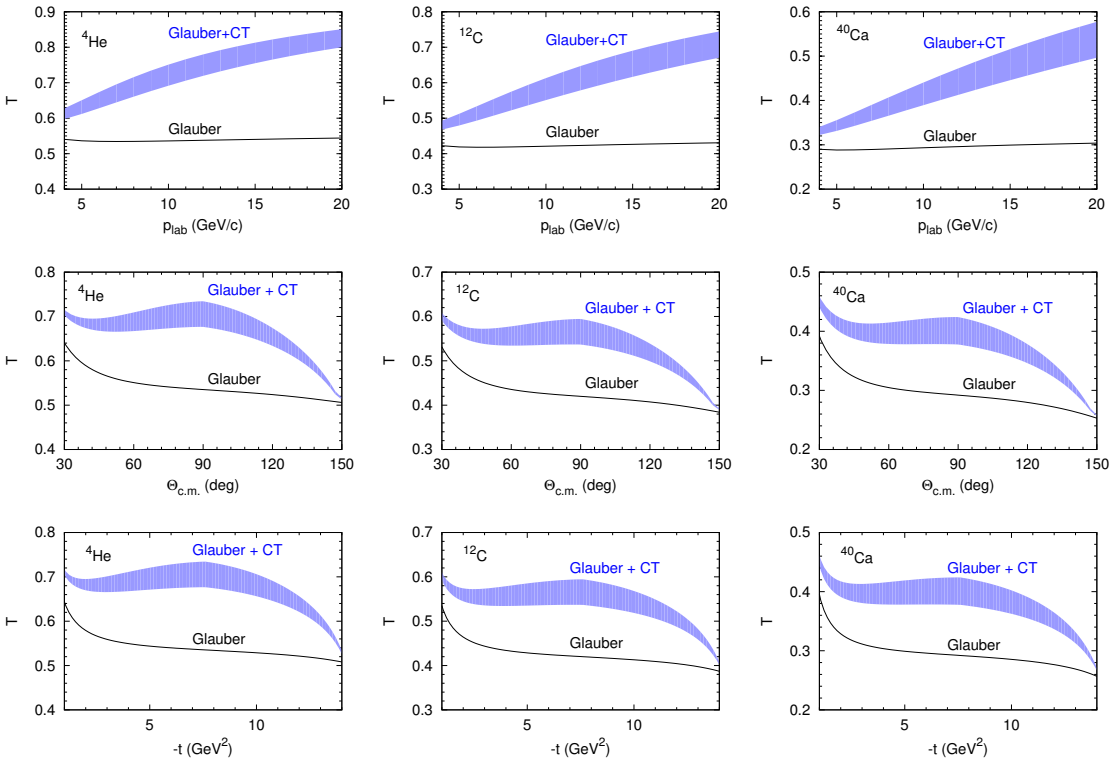

Figure 4: The transparency for the $A(\gamma, \pi^- p)$ reaction for ^{4}He (left column), ^{12}C (middle column), and ^{40}Ca (right column) shown as a function of the photon energy for a 90° c.m. scattering angle (top row), of c.m. scattering angle (middle row), and of momentum transfer (bottom row) for 9 GeV photons.

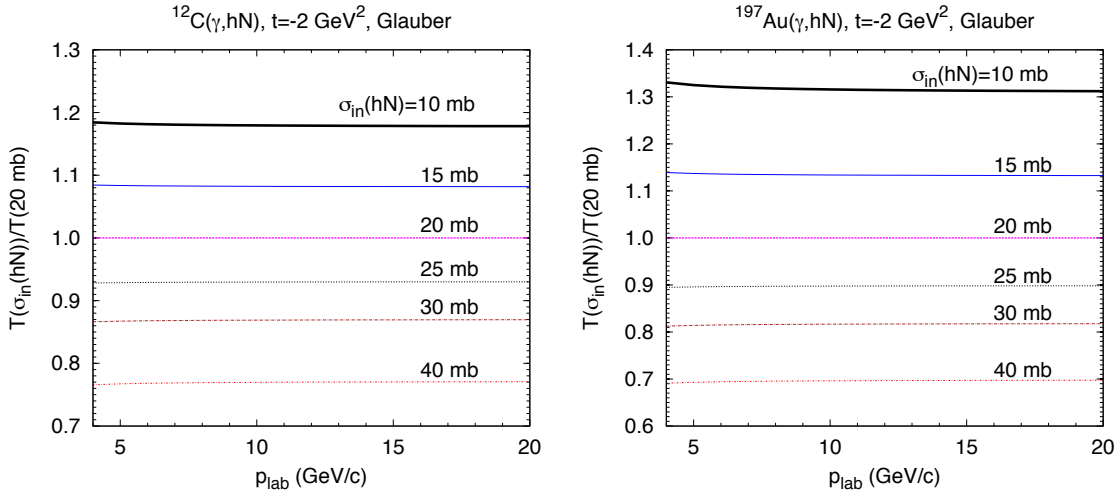

Figure 5: The ratio of the transparency for the $A(\gamma, hN)$ reaction to the transparency for the $A(\gamma, \pi^- p)$ reaction as a function of the photon momentum for different effective rescattering cross sections, σ_{hN}. The inelastic $\sigma_{\pi^- N}$ cross section was assumed to be 20 mb. The figure is taken from [9].

shown that SRCs in nuclei may have significant implications on the nuclear symmetry energy and neutron star structure [21, 22], the quark distributions in nuclei (the EMC effect) and the free (unbound) neutron structure [5, 6, 8, 23], energy sharing between protons and neutrons in asymmetric nuclear systems [24, 25] and more.

While the 6 GeV physics program at Jefferson-Lab revolutionized many aspects of our understanding of SRCs, there are still many aspects of correlations we do not yet understand. The main uncertainties relate to the interpretation of electro-induced quasi-elastic (QE) knockout reactions traditionally used to study SRCs. As the works relating SRCs to various other phenomena rely, to various degrees, on the standard interpretation of these data, it is important to test this interpretation by performing independent measurements using complementary probes, especially those whose reaction mechanisms and final state interactions (FSIs) are different than those of high-Q^2 electro-induced QE scattering.

The electro-induced QE scattering measurements were done at high-Q^2 kinematics (~ 2 GeV^2) and $x_B > 1$, where theoretical calculations indicate competing effects are expected to be small and/or well understood [6,7]. Possible competing effects include contributions from meson-exchange currents, isobar production and reabsorption, final-state interactions (FSI) and more; see Ref. [7] for a recent review.

We propose here to utilize the high intensity photon flux of Hall-D and the large acceptance of the GlueX spectrometer to perform a new generation of exclusive and semi-exclusive SRC studies using the $A(\gamma, X)$ and $A(\gamma, XN_{\rm recoil})$ reactions. Here X stands for the leading meson and baryon in the different channels listed in Tab. 1. $N_{\rm recoil}$ stands for a correlated recoil nucleon emitted in the case of photon-absorption on a nucleon that is part of a two-nucleon ($2N$) SRC pair.

The previous SRC studies using electron beams (i.e. virtual photon exchange) were mainly probing a proton in the SRC pair [24, 26–30]. The use of a real photon beam also allows probing, with high-precision, neutrons in SRC pairs through charged final states (e.g. $\gamma + n \to \pi^- + p$). In addition, the s^{-7} scaling of the exclusive photoproduction cross section enhances contributions from scattering off high-momentum forward-going nucleons in the nucleus that minimize s [18,19]. In the case of SRCs, this means that the high-momentum meson-baryon pair will preferentially go forward

while the recoil nucleon will be emitted in the backward direction. These 'parallel' kinematics are expected to significantly reduce and simplify FSIs [7] and are opposite to the 'anti-parallel' kinematics used in high-x_B electro-induced knockout measurements.

The use of exclusive photoproduction reactions, where all the energy of the photon (~ 9 GeV) is transferred to the active nucleon, introduces significantly different reaction mechanisms as compared to the electro-induced reactions. For example, meson exchange currents and isobar excitations are highly suppressed as they should lead to very different final states. The low-rate and large acceptance of the GlueX spectrometer will allow us to ensure the exclusivity of the final state, **enabling a stringent test for the universality of SRCs, their neutron-proton dominance, their c.m. momentum extraction, and more.**

The proposed measurement will study $A(\gamma, XN_{\text{recoil}})$ in nuclei and the deuteron. We will focus on hard reactions ($|t, u| > 2$) and cases where the missing momentum of X (sum of the meson and baryon momenta minus that of the photon) and the recoil nucleon momentum are larger than the nuclear Fermi momentum (~ 250 MeV/c), approximately equal in size, and opposite in direction. By comparing reactions off nuclei to reactions off deuterium in these kinematics, we can examine the dominance of np SRC pairs, the pairs' c.m. motion, and the relative abundance of SRC pairs in the measured nuclei.

2 Previous Measurements

2.1 CT at High Energies

At high energies, the phenomena of CT arises from the fact that exclusive processes on a nucleus at high momentum-transfer preferentially select the color singlet, small transverse size configuration, which then moves with high momentum through the nucleus. The interactions between the small transverse size configuration and other nucleons are strongly suppressed because the gluon emission amplitudes arising from different quarks cancel. This suppression of the interactions is one of the essential ingredients needed to account for Bjorken scaling in deep-inelastic scattering at small x_B [8].

CT at high energies was directly observed in the diffractive dissociation of 500 GeV/c pions into dijets when coherently scattering from carbon and platinum targets. The per-nucleon cross section for dijet production is parametrized as $s = s_0 A^a$, and the experiment found $a = 1.61 \pm 0.08$ [31], consistent with CT predictions of $a = 1.54$ [32]. These results confirm the predicted strong increase of the cross section with A, and the dependence of the cross section on the transverse momentum of each jet with respect to the beam axis (k_t) indicates the preferential selection of the small transverse size configurations in the projectile. Such experiments have unambiguously established the presence of small-size $q\bar{q}$ Fock components in light mesons and show that at transverse separations, $d \sim 0.3$ fm, pQCD reasonably describes small $q\bar{q}$-dipole-nucleon interactions. Thus, color transparency is well established at high energies and low x_B. However, these high-energy experiments do not provide any information about the appropriate energy regime for the onset of CT.

At intermediate energies, in addition to the preferential selection of the small-size configuration, the expansion of the interacting small-size configuration is also very important. At these energies, the expansion distance scales are not large enough for the small-size configuration to escape without interaction which, suppresses the color transparency effect [33–36]. The interplay between the selection of the small transverse size and its subsequent expansion determine the scale of the momentum and energy transfers required for the onset of CT. As mentioned, a major difference between photo-induced and electron-induced reactions is that, in the former, much greater energy is transfered relative to momentum, which can help disentangle the roles of freezing and squeezing.

The first attempt to measure the onset of CT at intermediate energies used the large-angle $A(p, 2p)$ reaction at the Brookhaven National Lab (BNL) [12, 37–39]. In these experiments, large-angle pp and quasielastic $(p, 2p)$ scattering were simultaneously measured in hydrogen and several nuclear targets, at incident proton momenta of 6–12 GeV/c. The nuclear transparency was extracted

from the ratio of the quasielastic cross section from a nuclear target to the free pp elastic cross section. The transparency was found to increase as predicted by CT, but only between 6–9.5 GeV/c; the transparency was found to decrease between 9.5 and 14.4 GeV/c. This decrease cannot be explained by models incorporating CT effects alone. Though not fully understood to date, this behavior is commonly attributed to a lack of understanding of the fundamental two-body reactions, which limits ones ability to relate the s, t scales for the onset of squeezing in different reactions. This situation raises doubts about our ability to study CT effects using such proton-induced QE scattering reactions.

In contrast to hadronic probes, weaker electromagnetic probes sample the complete nuclear volume. The fundamental electron-proton scattering cross section is smoothly varying and is accurately known over a wide kinematic range. Detailed knowledge of the nucleon energy and momentum distributions inside a variety of nuclei have been extracted from extensive measurements in low-energy electron scattering experiments. Therefore, the $(e, e'p)$ reaction is simpler to understand than the $(p, 2p)$ reaction, an advantage immediately recognized following the BNL $(p, 2p)$ experiments. A number of $A(e, e'p)$ experiments have been carried out over the years, first at SLAC [40, 41] and later at JLab [13, 42] for a range of light and heavy nuclei. In high Q^2 quasielastic $(e, e'p)$ scattering from nuclei, the electron scatters preferably from a single proton, which need not be stationary due to Fermi motion [43]. In the plane wave impulse approximation (PWIA), the proton is ejected without final state interactions with the residual $A-1$ nucleons. The measured $A(e, e'p)$ cross section would be reduced compared to the PWIA prediction in the presence of final state interactions, where the proton can scatter both elastically and inelastically from the surrounding nucleons as it exits the nucleus. The deviations from the simple PWIA expectation is used as a measure of the nuclear transparency. In the limit of complete color transparency, the final state interactions would vanish and the nuclear transparency would approach unity. In the conventional nuclear physics picture, one expects the nuclear transparency to show the same energy dependence as the energy dependence of the NN cross section. Other effects such as short-range correlations and the density dependence of the NN cross section will affect the absolute magnitude of the nuclear transparency but have little influence on the energy- (or Q^2-) dependence of the transparency. Thus, the onset of CT is expected to be manifested as a rise in the nuclear transparency as a function of increasing Q^2.

The existing world data rule out any onset of CT effects larger than 7% over the Q^2 range of 2.0–8.1 (GeV/c)^2 with a confidence level of at least 90%. As mentioned earlier, the onset of CT depends both on momentum and energy transfers, which affect the squeezing and freezing respectively. Since $A(e, ep)$ scattering measurements are carried out at $x_B = 1$ kinematics, they are characterized by lower energy transfers as compared to the momentum transfer (e.g. 4.2 GeV for $Q^2 = 8$ GeV^2). Existing data seem to suggest that a Q^2 of 8 (GeV/c)^2 with 4.2 GeV energy transfer is not enough to overcome the expansion of the small transverse size objects selected in the hard ep scattering process (i.e. freezing requirements are not met). An approved 12 GeV experiment will extend these studies to $Q^2 \sim 16$ GeV^2 [44]. Although, no unambiguous evidence for CT has been observed so far for nucleons from either $A(e, ep)$ or $A(p, 2p)$ reactions, it is expected to be more probable to reach the CT regime at low energy for the interaction/production of mesons than for baryons, since only two quarks must come close together and a since a quark-antiquark pair is more likely to form a small size object [45]. Indeed, pion production measurements at JLab reported evidence for the onset of CT [10] in the process $e + A \rightarrow e + p + A^*$. The pion-nuclear transparency was calculated as the ratio of pion electroproduction cross section from the nuclear target to that from the deuteron. As proposed here, the use of the deuteron instead of the proton helped reduce the uncertainty due to the unknown elementary pion electroproduction cross section off a free neutron and to uncertainties in the Fermi smearing corrections. The measured pion nuclear transparency shows a steady rise with increasing pion momentum for the $A > 2$ targets, and this rise in nuclear transparency versus p_π is consistent with the rise in transparency predicted by various CT calculations [46–48]. Although, all the calculations use an effective interaction based on the quantum diffusion model [33] to incorporate the CT effect, the underlying conventional nuclear physics is calculated very differently. The results

of the pion electroproduction experiment demonstrate that both the energy and A dependence of the nuclear transparency show a significant deviation from the expectations of conventional nuclear physics and are consistent with calculations that include CT. The results indicate that the energy scale for the onset of CT in mesons is ~ 1 GeV.

Electroproduction of vector mesons from nuclei is another excellent tool to investigate the formation and propagation of quark-antiquark ($q\bar{q}$) pairs under well-controlled kinematical conditions. Soon after the observation of the onset of CT in pion electroproduction, results from a study of ρ-meson production from nuclei at JLab also indicated an early onset of CT in mesons [11]. Previous ρ^0 production experiments had shown that nuclear transparency also depends on the coherence length, l_c, which is the length scale over which the $q\bar{q}$ states of mass $M_{q\bar{q}}$ can propagate. Therefore, to unambiguously identify the CT signal, one should keep l_c fixed while measuring the Q^2 dependence of the nuclear transparency. The CLAS collaboration at JLab measured the nuclear transparency for incoherent exclusive ρ^0 electroproduction off carbon and iron relative to deuterium [11] using a 5 GeV electron beam. An increase of the transparency with Q^2 for both C and Fe, was observed indicating the onset of CT phenomenon. The rise in transparency was found to be consistent with predictions of CT by models [49, 50] which had successfully described the increase in transparency for pion electroproduction. Therefore, the π and ρ electroproduction data also demonstrate an onset of CT in the few GeV energy range as shown in Figure 6. Both of these experiments will be extended to higher energies in future 12 GeV experiments [44, 51].

In the case of large momentum transfer exclusive photoinduced reactions, while the predicted effects are larger (Fig. 4) they were not studied in much detail. JLab experiment E94-104 searched for CT using the reaction $\gamma + n \to \pi^- + p$ [52]. The experiment used an untagged mixed electron and photon bremsstrahlung beam incident on a ^{4}He target and the Hall-A high-resolution spectrometers to measure π^- and p produced in the reaction. The momentum transfer was reconstructed assuming scattering off a mean-field neutron in ^{4}He leaving the residual system in the ground state of ^{3}He. Nuclear transparency was measured as a ratio of the pion photoproduction cross section from ^{4}He to that of ^{2}H. Figure 7 shows the extracted transparency as a function of the momentum transfer, $|t|$, for center-of-mass scattering angles of 70° and 90°. The results were compared to Glauber calculations with and without CT effects. As can be seen, the measurement did not have the required statistical and systematical accuracy to discriminate between the two calculations over the measured $|t|$ range. We propose, using the advantages of the GlueX spectrometer and the upgraded CEBAF 12 GeV electron beam, to add many more reaction channels, extend the measured $|t|$ range up to 10–12 GeV^2, and add heavier nuclei. While we will keep comparable uncertainties, for heavier nuclei and larger momentum transfers the expected effects are considerably larger, which significantly increases the discovery potential.

It should be pointed out that the rate of expansion/contraction of configurations involved in the interaction with nucleons is the same for the different reactions. Hence, in light of the successful description of CT for mesons, reliable estimate of space-time evolution effects were performed for other reactions with the conclusion that in the proposed kinematics for GlueX, CT is not washed out by the expansion/contraction effects due to the high photon energies used in the experiment.

2.2 SRC Studies using (e, epN) and $(p, 2pn)$ Reactions

Recent high-momentum-transfer triple-coincidence ^{12}C$(p, 2pn)$ and $A(e, e'pN)$ measurements (where $A =$ ^{4}He, ^{12}C, ^{27}Al, ^{56}Fe, and ^{208}Pb) [24, 26–30] indicated that nucleons in the nuclear ground state form nucleon pairs with large relative momentum and small center-of-mass (c.m.) momentum, where large and small are relative to the Fermi momentum of the nucleus (k_F). We refer to these pairs as short-range correlated (SRC) pairs. For missing-momenta (the initial momentum of the knocked-out nucleon prior to scattering, in the absence of re-interactions) in the range of 300–600 MeV/c, these pairs were found to dominate the nuclear wave functions, with neutron-proton (np) pairs nearly 20 times more prevalent than proton-proton (pp) pairs, and by inference neutron-neutron (nn) pairs.

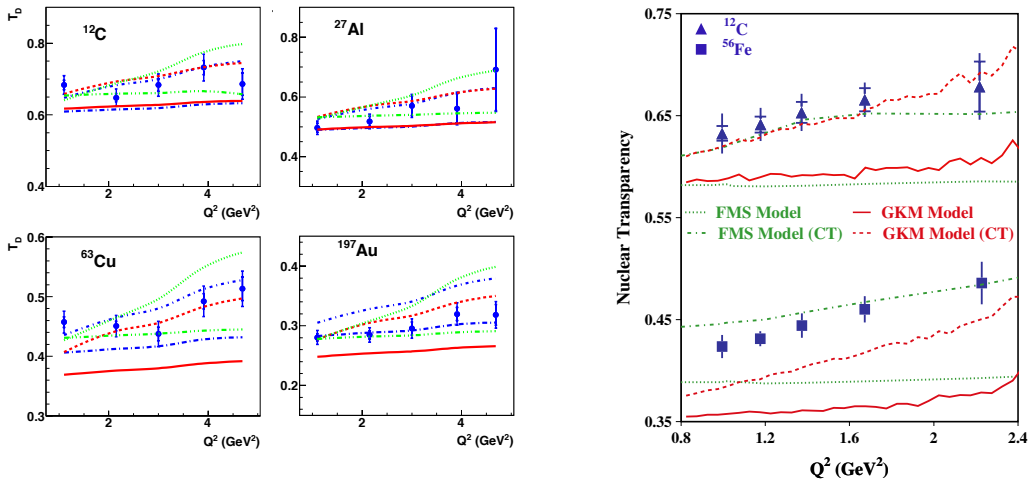

Figure 6: The two JLab experiments which show conclusive evidence for the onset of CT in meson electroproduction at intermediate energies. **(left panel)** Nuclear transparency vs Q^2 for ^{12}C, ^{27}Al, ^{63}Cu and ^{197}Au in the $(e, e'\pi^+)$ reaction. The inner error bars are the statistical uncertainties and the outer error bars are the statistical and point-to-point systematic uncertainties added in quadrature. The solid circles (blue) are the high-ϵ (virtual photon polarization) points, while the solid squares (red) are the low-ϵ points. The dashed and solid lines (red) are Glauber calculations from [46], with and without CT, respectively. Similarly, the dot-short dash and dot-long dash lines (blue) are Glauber calculations with and without CT from [47]. The dotted and dot-dot-dashed lines (green) are microscopic+ BUU transport calculations from [48], with and without CT, respectively. **(right panel)** Nuclear transparency as a function of Q^2 in the $(e, e'\rho^0)$ reaction. The curves are predictions of the FMS [49] (red) and GKM [50] (green) models with (dashed-dotted and dashed curves, respectively) and without (dotted and solid curves, respectively) CT. Both models include the pion absorption effect when the ρ^0 meson decays inside the nucleus. The inner error bars are the statistical uncertainties and the outer ones are the statistical and the point-to-point systematic uncertainties added in quadrature.

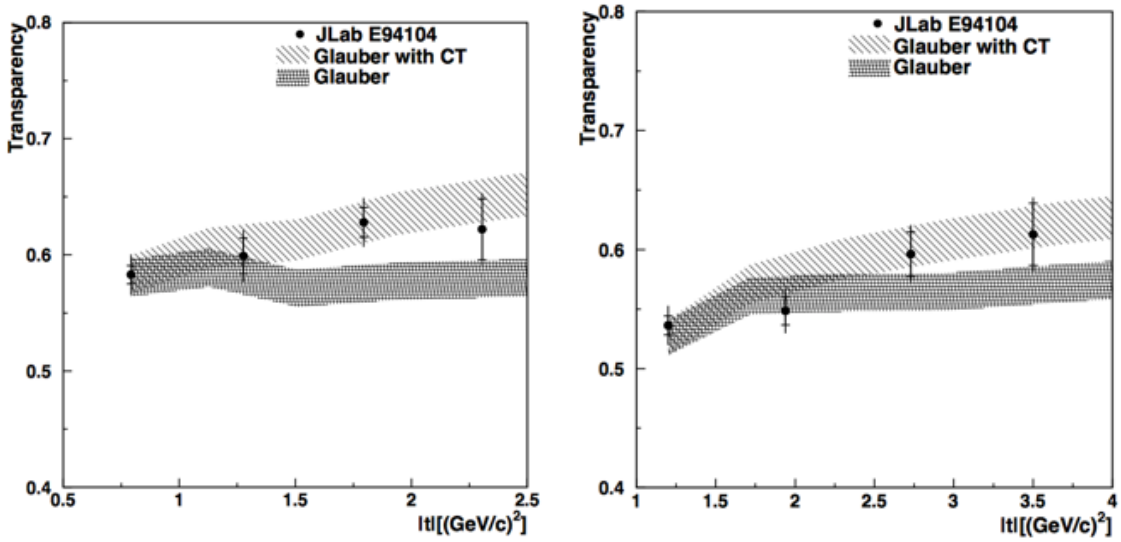

Figure 7: The measured transparency for the reaction ^{4}He$(\gamma, \pi^- p)$ for two c.m. scattering angles (70°-right, 90°-left). The measurements are compared to Glauber calculations with and without CT. See Ref. [49] for details.

See Figure 8.

These observations, combined with information deduced from (e, e') cross section ratios at high-Q^2 and $x_B > 1$ kinematics, imply that, in medium and heavy nuclei ($A \geq 12$), about 20% of the nucleons have momentum greater than the nuclear Fermi momentum. These nucleons have a deuteron-like one-body momentum distribution that is considered to be predominantly due to $2N$-SRC pairs, with about 90% being neutron-proton pairs and about 5% proton-proton and neutron-neutron pairs each. Due to their large momentum, they account for most (60–70%) of the kinetic energy carried by nucleons in nuclei. The microscopic interpretation of the observed proton-neutron pairs dominance is due to the strong dominance of the NN tensor interaction at the probed sub-fermi distances [53–55]. Follow-up experiments, described below, set out to measure the transition from the tensor dominant region to the nuclear repulsive core and map the influence of nuclear asymmetry.

In a recent publication, a simultaneous measurement of the ^{4}He$(e, e'p)$, ^{4}He$(e, e'pp)$ and ^{4}He$(e, e'pn)$ reactions at $(e, e'p)$ missing momenta from 400 to 830 MeV/c was reported [27]. The measurements were motivated by the attempt to study the missing momentum dependence of the isospin decomposition of $2N$-SRC as a proxy for a transition from the dominance of the tensor part to the short range repulsive (presumably scalar) part of the nucleon-nucleon interaction.

The experiment ran in Hall A using a 4.5 GeV electron beam and the two HRS spectrometers that detected the scattered electron and knocked out proton in coincidence with a kinematical missing-momentum coverage of 400–830 MeV/c. For highly correlated pairs, the missing momentum of the $A(e, e'p)$ reaction is expected to be balanced almost entirely by a single recoiling nucleon. A large acceptance spectrometer (BigBite), followed by a matching solid angle neutron detector (HAND), were used to detect correlated recoiling protons or neutrons. The results of these measurements are shown in Fig. 9 compared to a theory prediction based on a recent Variational Monte-Carlo (VMC) calculation. The overall upwards trend of the proton-proton to proton-neutron ratio is consistent with the theoretical expectation but the data is statistically limited.

Looking at neutron-rich asymmetric nuclei, a recent JLab data mining analysis project directly

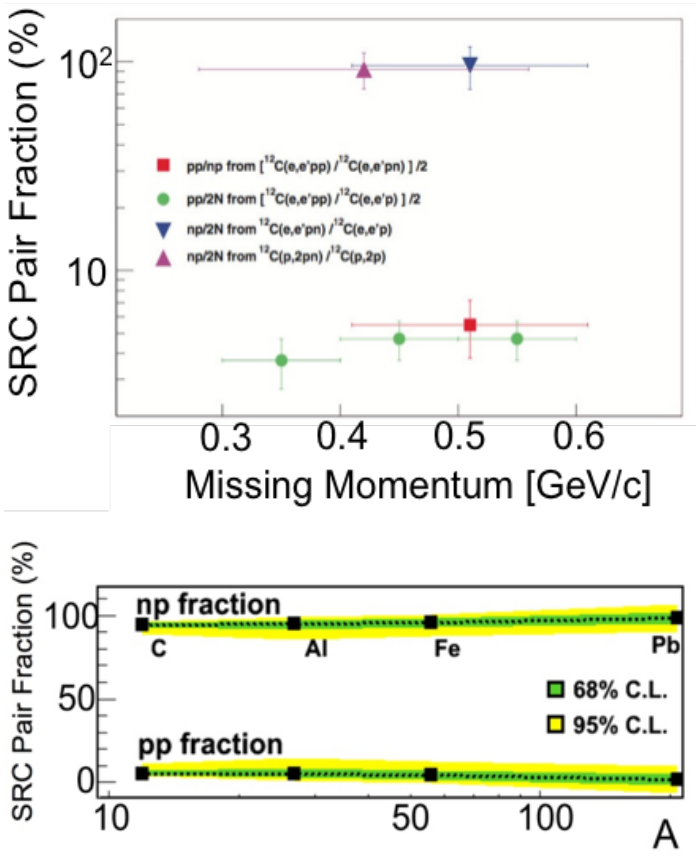

Figure 8: The fractions of correlated pair combinations in carbon as obtained from the ^{12}C$(e, e'pp)$ and ^{12}C$(e, e'pn)$ reactions measured at JLab [26, 30] as well as ^{12}C$(p, 2pn)$ data from BNL [28, 29]. (Bottom) The extracted fraction of neutron-proton and proton-proton pairs for nuclei ranging from ^{12}C to ^{208}Pb [24].

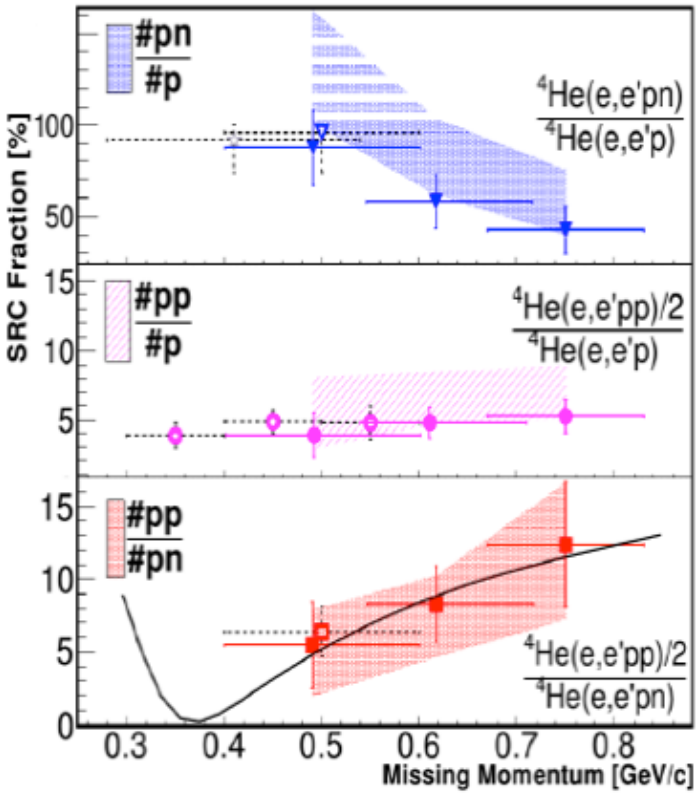

Figure 9: (Bottom) The measured ratios ^{4}He$(e,e'pp)/^4$He$(e,e'pn)$ shown as solid symbols, as a function of the ^{4}He$(e,e'p)$ missing momentum. The bands represent the data corrected for FSI to obtain the pair ratios; see Ref. [27] for details. Also shown are calculations using the momentum distribution of Ref. [56] for pairs with weighted-average c.m. momentum (solid black line). (Middle) The measured ^{4}He$(e,e'pp)/^4$He$(e,e'p)$ and extracted $\#pp/\#p$ ratios. (Top) the measured ^{4}He$(e,e'pn)/^4$He$(e,e'p)$ and extracted $\#pn/\#p$ ratios. The ratios for ^{12}C are shown as empty symbols with dashed bars. The empty star in the upper panel is the BNL result [28, 29] for ^{12}C$(p,2pn)/^{12}$C$(p,2p)$.

studied the isospin decomposition of the high-momentum tail of the nucleon momentum distribution in nuclei by simultaneously measuring hard QE electron scattering off protons and neutrons in nuclei. The experiment measured the $A(e,e'p)$ and $A(e,e'n)$ reactions respectively for $A =$ ^{12}C, ^{27}Al, ^{56}Fe, and ^{208}Pb nuclei. The simultaneous measurement of both proton and neutron knockout is a unique feature of this work that allows to directly compare their properties with few assumptions. The measurement was done in two kinematical settings, one corresponding to electron scattering off a nucleon from an SRC pair ($k > k_F$), the other from a nucleon from the mean field ($k < k_F$). Using these event samples, the $A(e,e'n)/A(e,e'p)$ cross section ratio for each of the kinematics was extracted; see Figure 10.

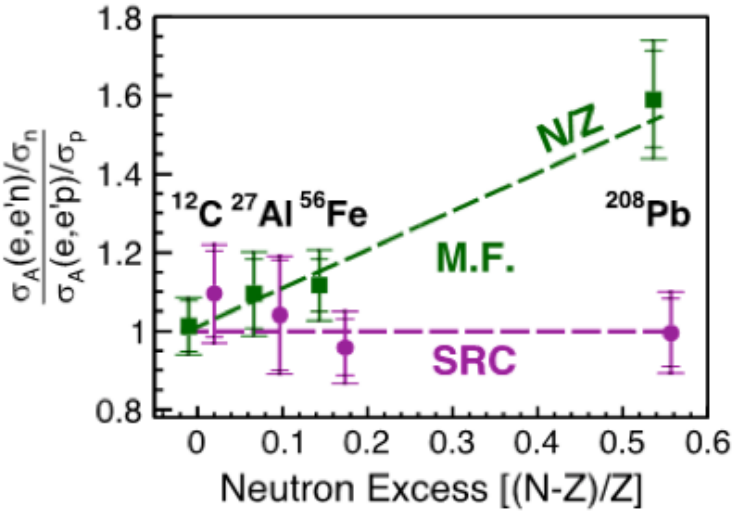

Figure 10: The $A(e,e'p)/A(e,e'n)$ reduced cross section ratio mean-field (green) and SRC (purple) events (left). The dashed lines are simple model predictions for the N/Z neutron excess dependence of the mean-field nucleons and the independence of neutron excess of the SRC nucleons.

For the symmetric ^{12}C nucleus, the SRC and mean-field neutron-to-proton knockout reduced cross section ratios: $[^{12}\mathrm{C}(e,e'n)/\sigma_{e^-n}]/[^{12}\mathrm{C}(e,e'p)/\sigma_{e^-p}]$ (i.e. measured cross sections divided by the known elementary electron-proton σ_{e^-p} and electron-neutron σ_{e^-n} cross sections) are each consistent with unity. For the other measured nuclei, the n/p mean-field reduced cross section ratios grow approximately as N/Z, as expected from simple nucleon counting. However, the SRC ratios are consistent with unity for all measured nuclei. This implies that the observed constant ratio is caused by np-pair dominance at high-momentum and thus, we find that there is an equal number of high momentum protons and neutrons in asymmetric nuclei, even though they hold disproportionally more neutrons than protons.

As mentioned, the results from these measurements and others are the basis for various theoretical and phenomenological studies addressing a wide variety of topics, from understanding the many-body wave function, to possible implications for the nuclear symmetry energy and neutron star structure, to quark distributions in nuclei (the "EMC effect") and the free (un-bound) neutron structure, to energy sharing between protons and neutrons in asymmetric nuclear systems and more.

However, the interpretation of these data relies on various calculations of reaction mechanisms that should be experimentally verified. The proposed study of SRCs in d, ^{4}He, ^{12}C, and ^{40}Ca, using exclusive photo-production reactions with real photons, will complement the above-mentioned studies and yield stringent constraints on possible reaction mechanisms that could complicate the interpretation of the data. If the reaction mechanisms at these high momentum transfer reactions

(Q^2, $|t|$, $|u| > 2$ GeV^2) are indeed understood to the expected level, we should be able to confirm the observed neutron-proton dominance and A-dependence of the number of SRC pairs through this experiment. Furthermore, the proposed measurement will be able to make large improvements in precision, as it will surpass previous measurements in statistics.

3 The Proposed Measurement

3.1 Kinematics

The kinematical distributions and expected event rates were simulated for the pion-proton photoproduction reaction off a neutron bound in a nucleus, $A(\gamma, \pi^- p)$, using a dedicated Monte-Carlo event generator. In this section, we present the simulation method and show the resulting kinematical distributions.

The simulation uses an incoming photon with energy sampled from the tagged photon spectra obtained from the standard GlueX simulation software (Fig. 11). The momentum distribution of the nucleons in the nucleus has two components: a mean-field region that spans low momentum (up to k_F) and account for 80% of the nucleons and an SRC region that spans high momentum (from k_F and up) and account for 20% of the nucleons. The SRC-pairs are modeled using a three-dimensional Gaussian center of mass momentum distribution with width (sigma) of 140 MeV/c [27,28,30,57,58] In the case of the deuteron, the AV18 momentum distribution was used.

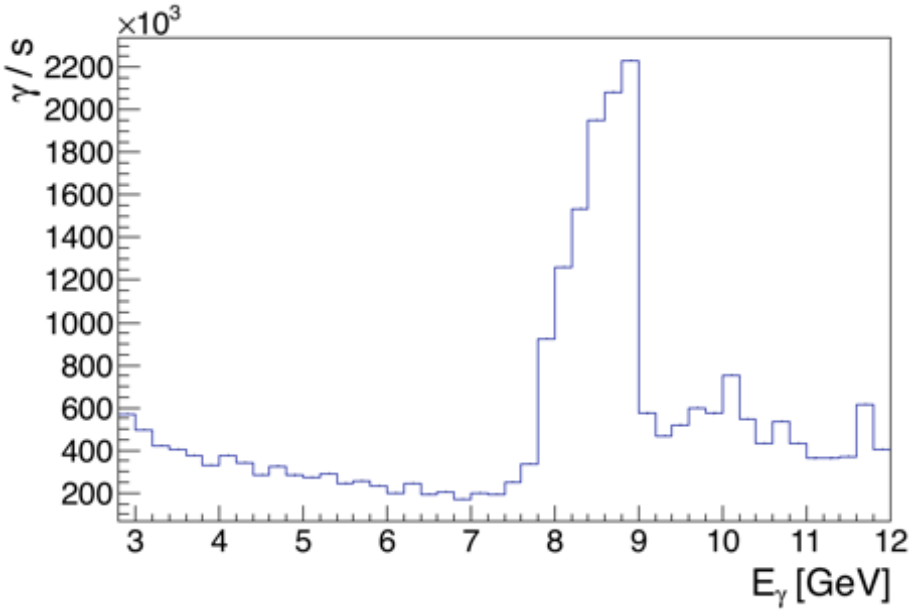

Figure 11: The energy distribution for the incoming photon beam hitting the GlueX target assuming a 5 mm diameter collimator. The distribution is normalized to a flux of 2.5×10^7 photons/s in the beam energy range 7.5 GeV $< E_{\text{beam}} <$ 11.7 GeV.

The cross section for the $\gamma + n \to \pi^- + p$ reaction was calculated based on the experimental data for 90° scattering in the c.m. with $s > 6.25$ GeV^2 assuming factorization of the s and c.m. angle dependence, i.e., $\frac{d\sigma}{dt}|_{\theta_{c.m.}} = (C \times s^{-7}) \times f(\theta_{c.m.})$, where C is a free fit parameter and f was extracted from the SLAC data assuming $f(90°) = 1$ [59], see Fig. 12.

The scattering was performed in the c.m. frame of the bound nucleon and gamma beam for

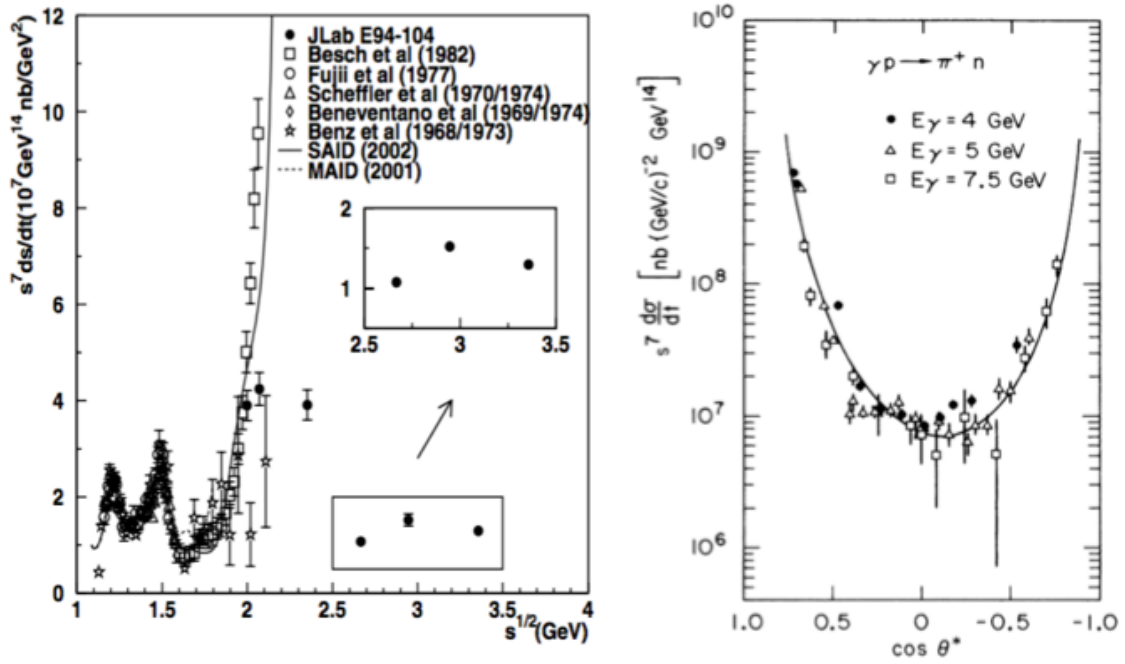

Figure 12: The s dependence of the photonuclear cross section at 90° in the c.m. (left) and its dependence on the c.m. angle (right). We extract the cross section by fitting the s dependence at high-s, after the low-s oscillations appear to be over. Figures were adapted from [59].

scattering angles of 40°–140°. Hard reaction kinematics where enforced by requiring $|t, u| > 2$ GeV^2. We note that the rate for lower momentum transfers is very high and within the GlueX acceptance. Figures 13 and 14 show the kinematical distributions for the final state particles respectively for interactions of the gamma with a mean-field nucleon and an SRC nucleon. For the case of SRC pairs breakup, the distribution of the correlated recoil proton is shown in Fig. 15. As mentioned, the backward peak of the recoil proton is due to the s^{-7} weighting of the cross section that prefers interactions with forward going nucleons which, in the case of SRCs, enforce the recoil nucleon to be emitted in a backward direction. We note that the resulting kinematical distributions are not very different from those obtained for scattering off stationary nucleons, which is what GlueX was designed to do.

The simulation results were compared to a simple, back-of-the-envelope calculation for the reaction cross section. This calculation is explained in Appendix A. The back-of-the-envelope result is within 20% of the simulation, giving us confidence in the validity of our simulation.

3.2 Optimization of the Tagged Gamma Energy Range

The Hall-D beam allows for a broad distribution of tagged photons on the target (Fig. 11). Due to the coincidental rate limitation of the Hall-D tagger we cannot consider the full gamma spectrum and should focus on a given energy range. Fig. 16 shows the correlation of $|t|$ and the beam-energy. As we are largely interested in large $|t|$ reactions, we choose to focus the tagger at the coherent peak, with gamma energies of 8 GeV $< E_{\text{beam}} <$ 9 GeV.

The number of photons in the coherent peak is regulated by the size of the collimator: a wider collimator ensures more coherent photons to hit the target. A collimator diameter of 5 mm was found to be optimal, as it allows measuring all the coherent photons with minimal 'background'

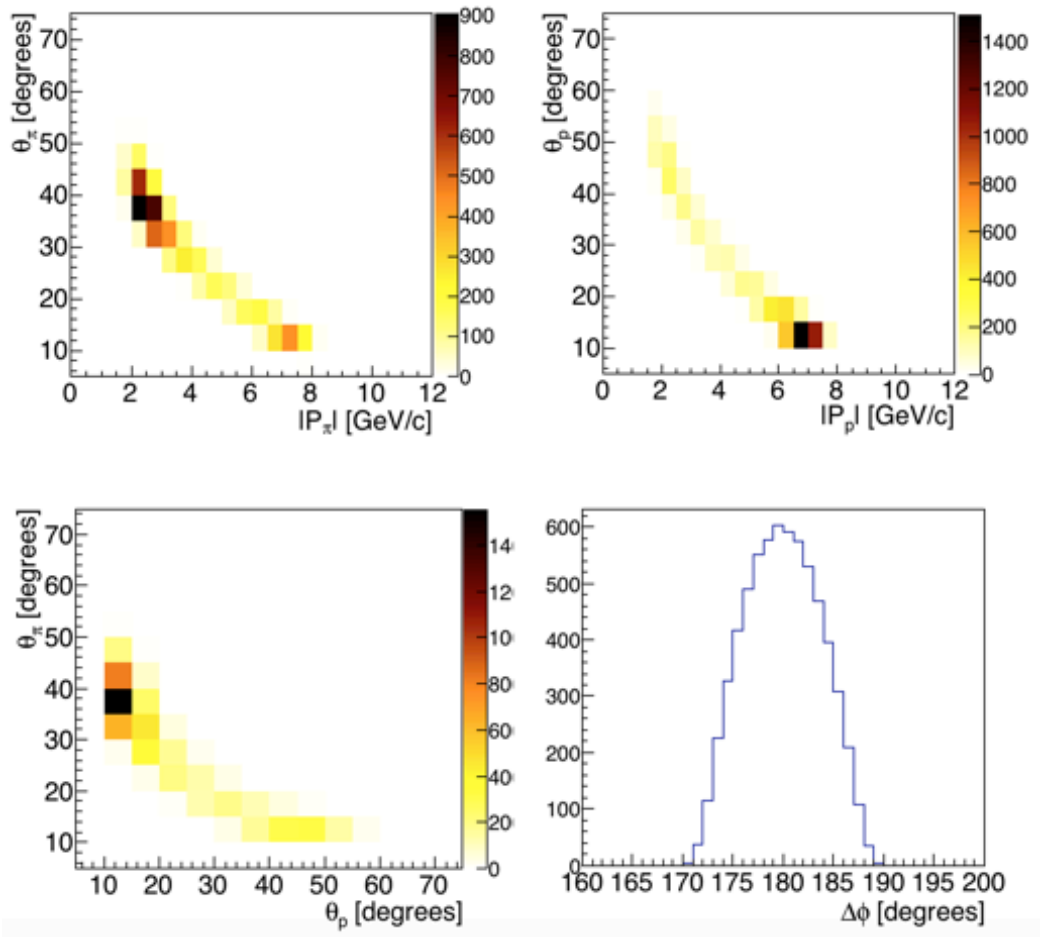

Figure 13: Kinematical distributions for the final state particles of the $\gamma + n \to \pi^- + p$ reaction for the MF regime ($P_{\text{miss}} < 0.25$ GeV/c).

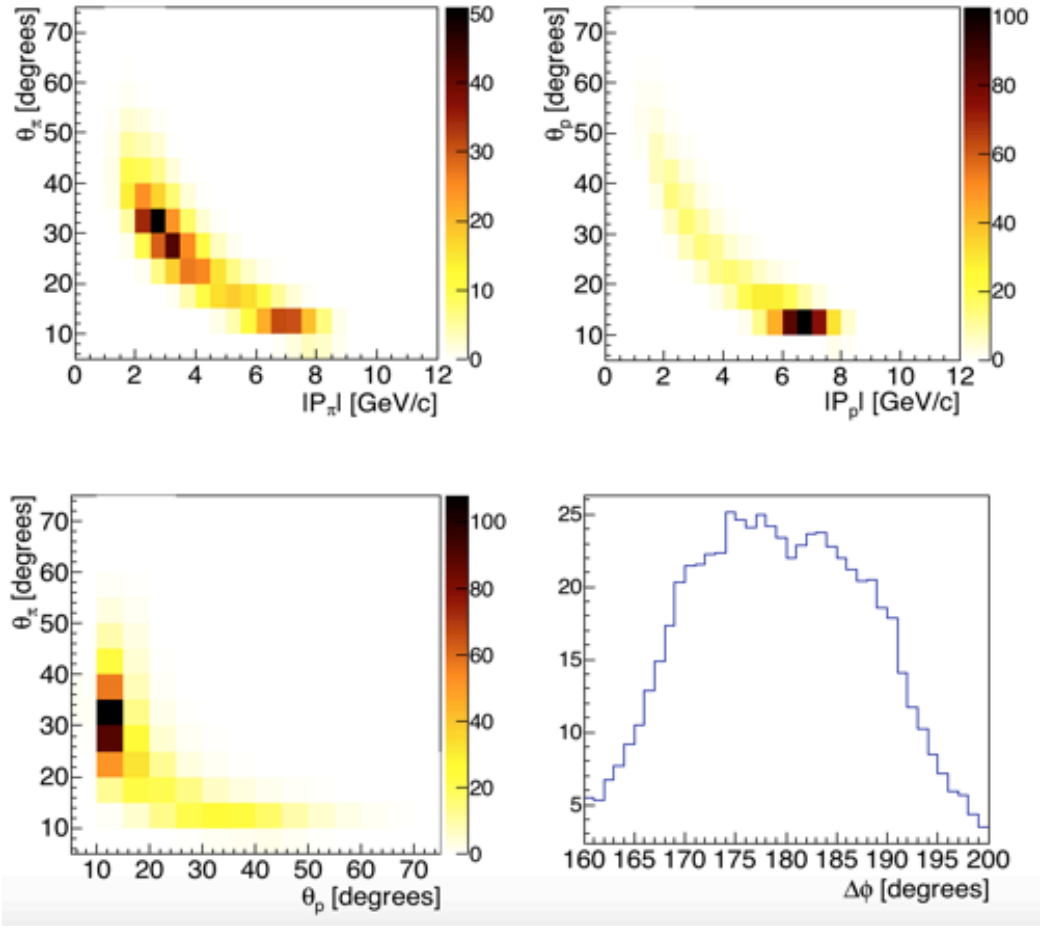

Figure 14: Same as Fig. 13 for the SRC regime ($P_{\rm miss} > 0.25$ GeV/c and $q_{\rm recoil} < 160°$).

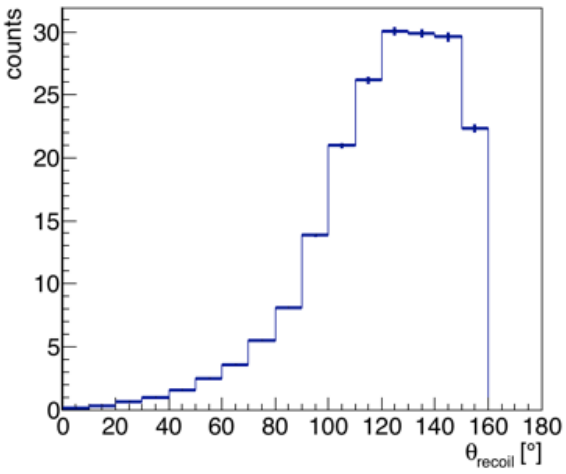

Figure 15: The angular distribution of the recoil nucleon when scattering off an SRC pair in the nucleus.

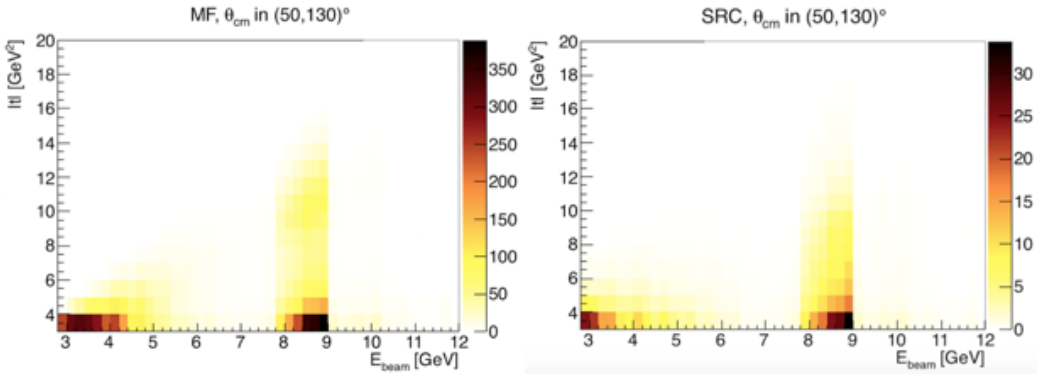

Figure 16: The momentum transfer $|t|$ as a function of the photon beam energies for two regimes of event selection: MF on the left and SRC on the right. The center of mass angle is in the range between 50° and 130°.

from low energy photons. Smaller collimator will reduce the high-energy gamma flux and larger collimator will increase the low energy background (leading to larger EM and neutron backgrounds) without improving the high-energy gamma flux.

The factors limiting the beam luminosity are the coincidental rate in the tagger and the electromagnetic background level in the GlueX spectrometer. The tagger coincidental rate for a photon flux on the target of 2×10^7 photons/s and RF time of 4 ns is expected to be about 18%.

To be conservative, the rate calculations presented below (and kinematical distribution presented above) are done for photon beam energies in the 8 GeV $< E_{\text{beam}} <$ 9 GeV range alone.

3.3 Final State Particle Detection

The efficiencies for the reconstruction of final state particles (i.e. meson-baryon pair and, in the case of SRC breakup, also the recoil proton) were simulated using the Geant-based GlueX simulation chain for the event generator described in the previous section. Fig. 17 shows the simulated detection efficiency for each particle separately. The average efficiency for the simultaneous reconstruction of the proton and a pion was found to equal 64%.

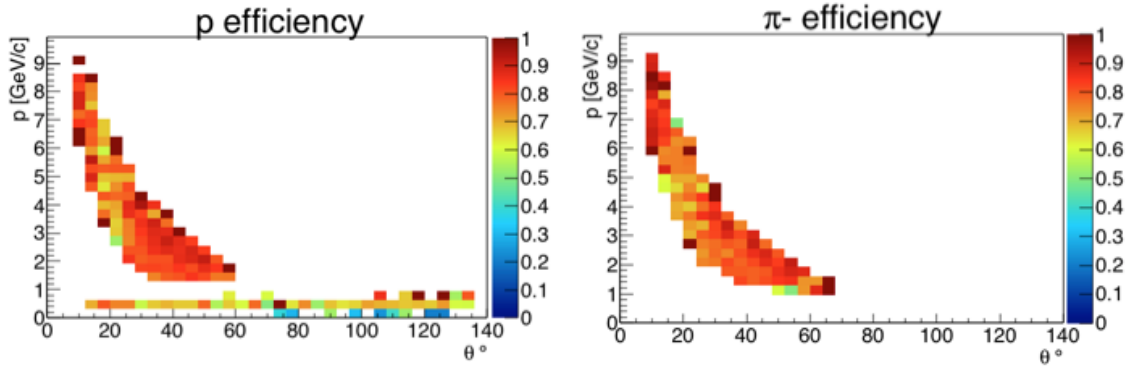

Figure 17: The reconstruction efficiency for the charged tracks coming from the reaction $\gamma n \to \pi^- p$. On the left panel the low momentum band is due to recoil protons form SRC pairs breakup.

Based on the current GlueX data reconstruction efficiencies, we expect that more complex final

states will have varying detection efficiencies reaching down to 30% for rho mesons. The total detection efficiency for the reaction $\gamma + n \to \rho^- + p$ is therefore assumed to be $0.9 \times 0.3 = 27\%$.

In the case of SRC pairs breakup, one should also take into account the detection efficiency of the recoil proton in the backward hemisphere. Figure 17 also shows the simulated detection efficiency of the recoil proton for the case of SRC pair breakup. Fig. 18 shows the detailed acceptance and detection efficiency for recoiling protons for 3 different vertex positions—at the center and two ends of the 30 cm long hydrogen target. As can be seen, the detection efficiency is very high up to 140° in the lab and can extend up to 160° when the target is placed downstream. Fig. 19 shows the vertex reconstruction resolution, showing we can separate solid target foils with a distance of ~ 1 cm which is more than enough to separate different foils in the case of ^{12}C and/or ^{40}Ca targets.

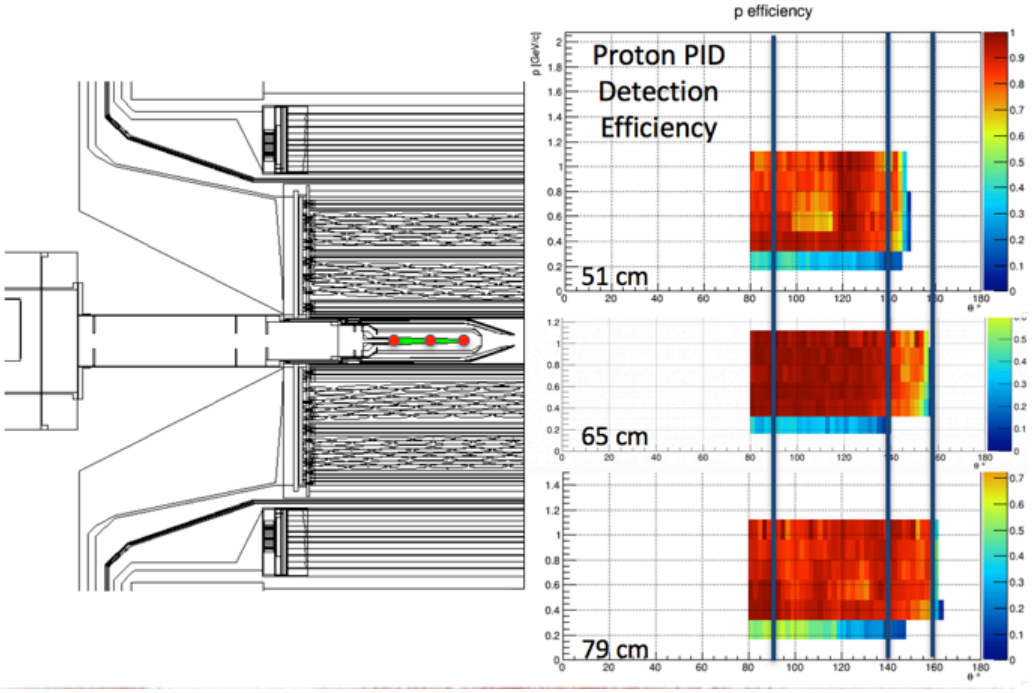

Figure 18: The detection efficiency for recoiling protons in GlueX as a function of the recoil angle and momentum for 3 different vertex locations.

3.4 Expected Rates

The rate calculations were done for the $\gamma + n \to \pi^- + p$ and $\gamma + n \to \rho^- + p$ reactions, using the simulation presented in section 3.1. We choose these two reactions as they have the smallest and largest cross sections respectively, of the reactions listed in table 1 which makes them a good representative of the various expected rates.

We assume a total of 40 beam days with a photon flux of 2×10^7 s^{-1} (compared to the nominal GlueX photon flux of 10^8 photons/s) and four targets: D, ^{4}He, ^{12}C and ^{40}Ca. Based on the acceptance simulations presented above, we assume 80% detection efficiency for each of the leading baryon and meson and 65% for the recoil nucleon. We assume the nominal nuclear attenuation effect reduces the total cross section as $A^{-1/3}$. Table 2 lists the parameters for the chosen targets. The factors limiting the event rates are the following:

- GlueX detector capabilities (maximum possible gamma flux on target)

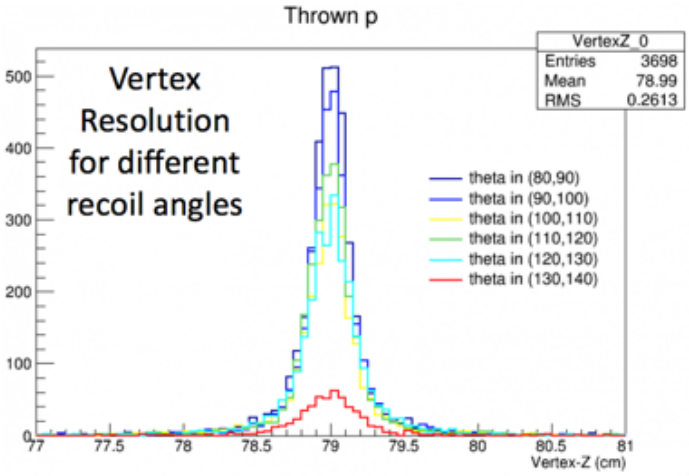

Figure 19: The vertex reconstruction resolution for recoiling protons at various recoil angles.

- Electromagnetic background in the GlueX spectrometer
- Tagger coincidental rate
- Neutron background

Presently, GlueX is operating with a 30 cm long liquid hydrogen (LH) target (3.4% radiation length, X_0). For the nominal beam flux on the target of 10^8 photons/s the electromagnetic background is reaching its upper limit. In order to comply with the electromagnetic background limits, we assume the carbon target thickness to be 7% X_0 (note that unlike for hydrogen, for nuclei there are 2 nucleons for each electron in the target. Therefore, for EM background estimations, 7% X_0 on nuclei is equivalent to 3.5% X_0 on hydrogen). The radiation lengths for liquid hydrogen, deuterium, and helium are similar. The use of nuclear targets will increase the slow neutron background that can induce some damage to GlueX detector components such as the SiPMs. Table 2 shows an estimate of the neutron background, done in collaboration with Hall D staff, based on JLAB-TN-11-005. GlueX was designed to handle one year of LH running with a photon flux of 10^8 photons/s. While the proposed gamma flux for this measurement is smaller by a factor of 5, detailed estimations by the Radcon group, backed with relevant measurements, show that replacing the LH target with ^{4}He will increase the neutron background by a factor of 4–5 (depending on the exact location). This implies that the neutron background for ^{4}He target in our running conditions will be similar to the GlueX design specifications. The estimated neutron backgrounds for all targets are shown in table 2, and are calculated from the Radcon ^{4}He estimate and their reported A-dependence. For reference, the table includes the GlueX LH target under nominal running conditions, i.e. 10^8 photons/s. The background rates for the other targets take into account the five-fold reduced gamma flux for the proposed experiment. While this background estimation procedure takes into account the main differences coming from nuclear targets relative to LH, the deuteron backgrounds could be somewhat higher. Given the very short deuteron beam time (table 3) this should not be an issue with regard to integrated demage.

Table 3 lists the expected events rate and beam time for each target for $|t, u| > 2$ GeV^2 for mean-field and SRC events separately. For Deuterium, as we use the AV18 distribution, the distinction is based on the initial momentum of the nucleon that the gamma interacted with (above or below 250 MeV/c). Figure 20 shows the expected count rate of various $|t|$ bins for Deuterium and ^{12}C for mean-field events. The statistics for $|t| < 2$ (GeV/c)^2 is rich, allowing to map the transition between

Table 2: Parameters for the proposed targets. The current GlueX liquid hydrogen target (LH) is shown for comparison. (*) The neutron flux for the LH target is taken under assumption of the nominal flux of 10^8 photons/s in the coherent peak.

Target	Thickness [cm] / % X_0	Atoms/cm^2 for the given target thickness	EM bkg. rel. to GlueX	Neutron bkg. rel. to GlueX
D	30 / 4.1	1.51×10^{24}	0.5	1.3
^{4}He	30 / 4	5.68×10^{23}	0.5	1
^{12}C	1.9 / 7	1.45×10^{23}	1	0.8
^{40}Ca	0.73 / 7	1.70×10^{22}	1	0.3
LH	30 / 3.4	1.28×10^{24}	1	1*

Table 3: Event rates estimation. See text for details.

Target	$\gamma + n \to \pi^- p$		$\gamma + n \to \rho^- p$		PAC Days
	MF	SRC	MF	SRC	
D	13,600	750	57,000	3,000	5
^{4}He	13,000	670	54,500	2,800	8
^{12}C	7,400	2,300	31,000	9,500	10
^{40}Ca	2,600	840	10,900	3,500	14
Calibration, commissioning, and overhead:					3
Total PAC Days:					40

different transparency regimes. Other nuclei have the same $|t|$ dependence and the expected count rate per bin can be scaled based on the total number of events listed in Table 3. We have chosen to distribute the beam time between the different targets so as to obtain comparable discriminating power for transparency studies and scaling of SRC pairs; the larger nuclei have larger predicted effects and therefore fewer statistics are needed to observe them at similar levels of significance.

Fig. 21 and Fig. 22 show the expected results for the color transparency and photon transparency for the $\gamma + n \to \pi^- + p$ reaction. Other reactions from table 1 will have comparable or better discriminating power. We note that by taking ratios for nuclei relative to deuterium we minimize many of the theoretical systematical uncertainties and are dominated by the beam flux and target densities. Both are expected to be known to better than 3% which is what we assume for the overall systematical uncertainty which is included in Fig. 21 and Fig. 22.

Fig. 23 shows the photon transparency for the $\gamma + n \to \pi^- + p$ at $\theta_{cm} = 90^\circ$ relative to that of ^{4}He as a way of highlighting the differences in A-dependence of the point-like and vector-meson regimes. The sensitivities at other scattering angles and in other reactions are expected to be comparable or better. This will allow a detailed mapping of the transition between the two regimes.

For SRC studies, while the rates are modest they are in fact comparable, and even higher, per reaction as compared to the 6 GeV measurements done in Hall A and B. Therefore, the cross section ratios for scattering off nuclei relative to deuterium, in SRC kinematics, will allow us to test the observed *np*-dominance and extract the relative number of SRC pairs in the measured nuclei with $< 4\%$–10% accuracy. This data will therefore improve our understanding of SRCs and help to reduce interpretation uncertainty in a unique way un-matched by any other measurement that can

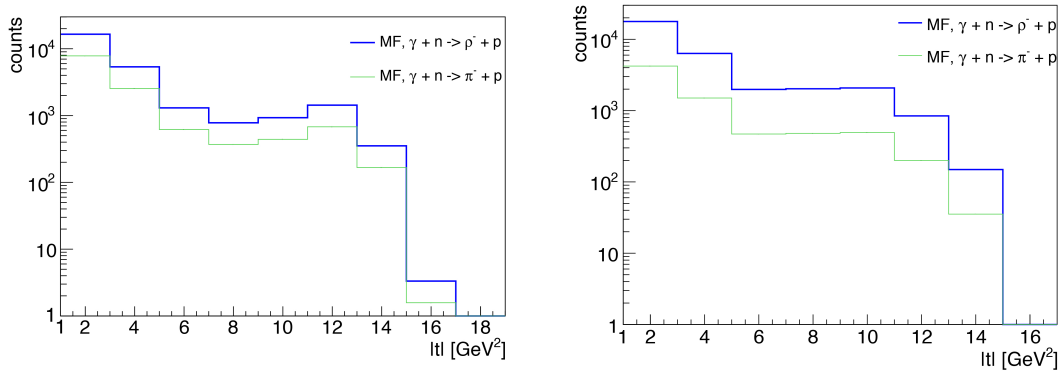

Figure 20: The expected count rate for 10 days running as a function of $|t|$ for Deuterium (left) and ^{12}C (right) targets in mean-field kinematics for two different reactions.

be performed at JLab.

4 Complimentary Experiments at JLab

The goals of our proposed measurement run complimentary to those of several other approved JLab 12 GeV experiments, which will be described in ths section.

Color transparency for mesons, hints of which were seen in the JLab 6 GeV program [10], will be studied at high-Q^2 in two upcoming 12 GeV electron scattering experiments: E12-06-106 [51] and E12-06-107 [44]. While these experiments are complimentary to our proposed CT measurement, we point out that our measurement is sensitive to CT for baryons as well. The large number of different final states we consider will allow us to map out the spin and isospin dependence of CT.

E12-06-107 will also measure color transparency in for protons, which compliments our baryonic CT measurements. A significant difference between this measurement and ours comes from the use of photon-induced reactions, which will generally have larger energy transfer (and thus greater "freezing" of PLCs) than the majority of the kinematic space probed by E12-06-107.

E12-11-112 [60] and E12-14-011 [61] are two upcoming Hall A measurements that will measure asymmetries between the mirror nuclei ^{3}H and ^{3}He to study isospin-dependent effects in SRCs, and thus are complimentary to our proposed SRC program. The interpretation of these experiments depends on the general framework for our understanding of SRCs, FSIs, etc. in electron-induced pair break-up, which our proposed measurement will attempt to validate with the new method of photo-induced reactions.

E12-11-003A [62] and E12-11-107 [63] will both test the role that highly-virtual nucleons play in the EMC effect by looking at recoil-tagged F_2 structure functions of bound nucleons in deuterium. As discussed in section 1.2, the theoretical framework of PLCs suggests that both color transparency and the EMC effect have a common origin. Both these experiments and our proposed measurement will have complimentary roles in constraining that framework and in understanding the origin of the EMC effect.

5 Summary

We propose to measure the $A(\gamma, X)$ and $A(\gamma, XN_{\text{recoil}})$ reactions (where X represents a wide range of meson-baryon final states) for $A =^2$H, ^{4}He, and ^{12}C using the maximum possible rate of coherent

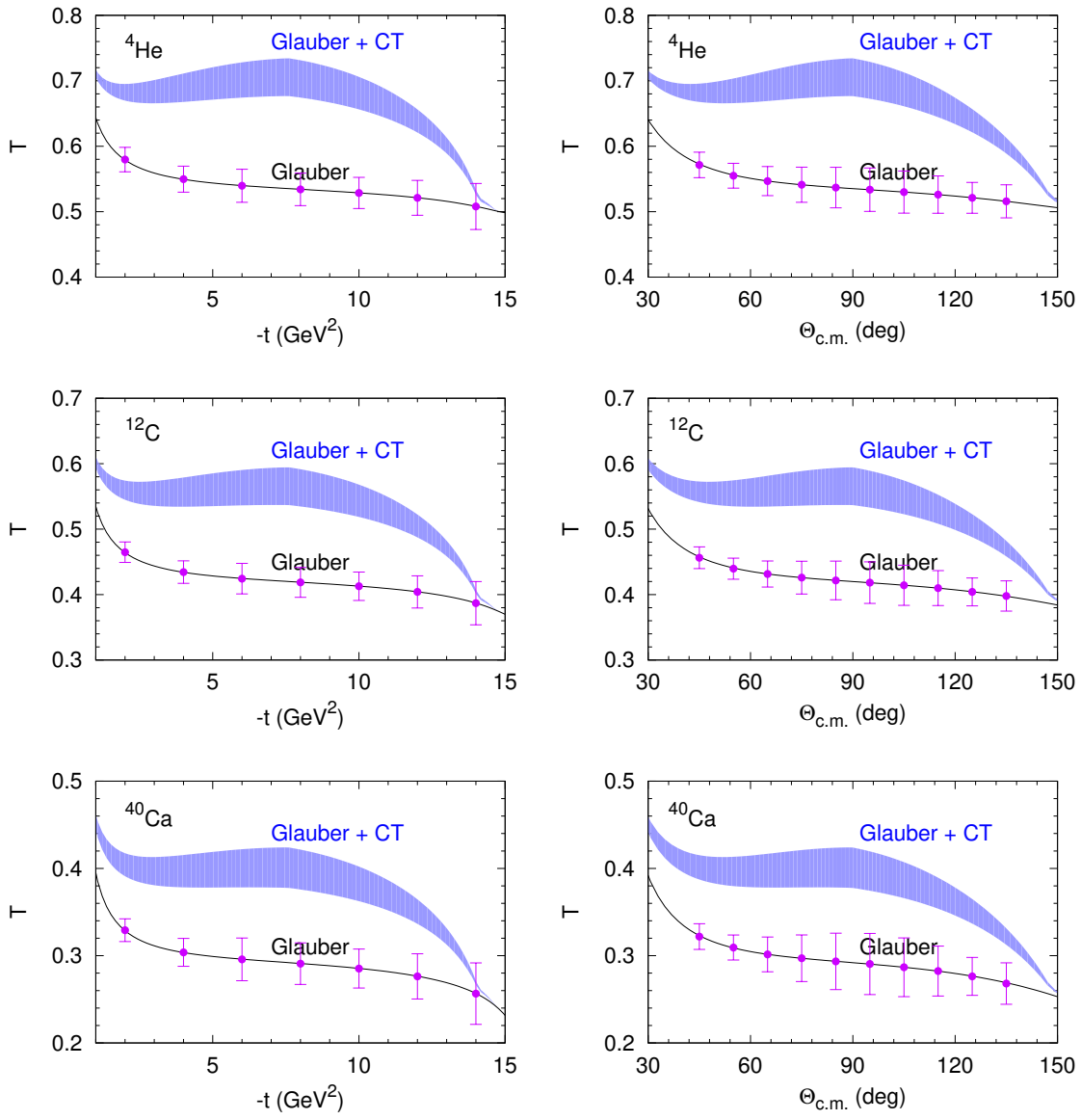

Figure 21: Expected uncertainties (statistical + systematical) for the measurement of the $\gamma + n \to \pi^- + p$ reaction off ^{4}He (upper row), ^{12}C (middle row), and ^{40}Ca (bottom row).

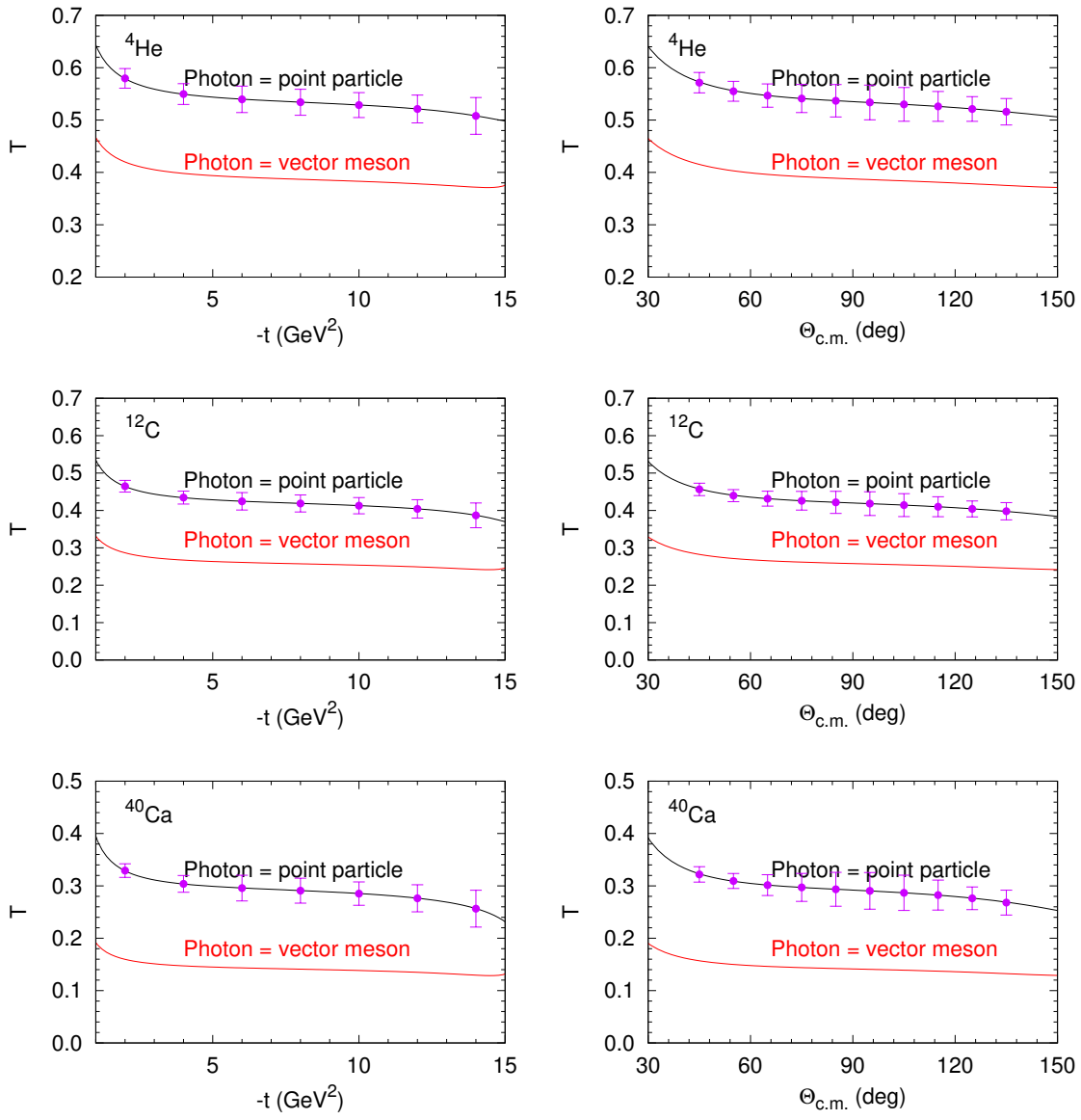

Figure 22: Expected uncertainties (statistical + systematical) for the measurement of the $\gamma + n \to \pi^- + p$ reaction off ^{4}He (upper row), ^{12}C (middle row), and ^{40}Ca (bottom row).

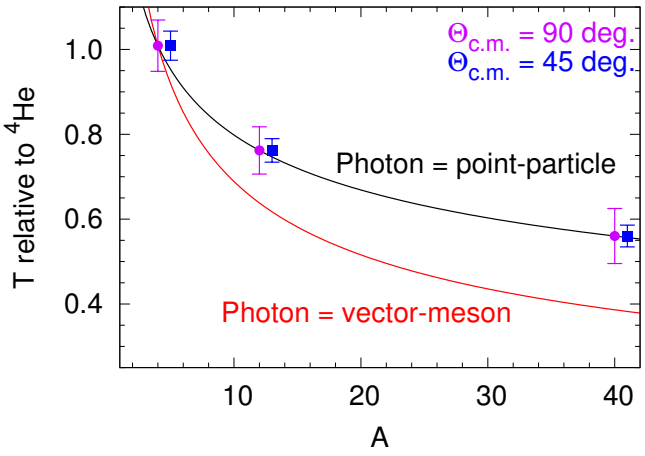

Figure 23: Expected uncertainties (statistical + systematical) for the measurement of the $\gamma + n \to \pi^- + p$ relative to ^{4} He. The curves are the same power law fits as in Fig. 3. The data points at $\theta_{cm} = 90°$ (magenta) have the largest expected uncertainties of any bin, while the data points at $\theta_{cm} = 45°$ (blue) have the smallest.

bremsstrahlung photons at $E_e = 12$ GeV (i.e. 8–9 GeV photons).

The data will be used to address the following issues:

- Transition from resolved to unresolved photon dominance.
- CT for different particles and reactions.
- The reaction of Quasi-Elastic scattering of a single nucleon in SRC pair.

We estimate this measurement will require a total 40 days at 12 GeV.

References

[1] "The 2015 Long Range Plan for Nuclear Science." http://science.energy.gov/np/nsac/.

[2] D. Dutta, K. Hafidi, and M. Strikman, "Color Transparency: past, present and future," *Prog. Part. Nucl. Phys.*, vol. 69, pp. 1–27, 2013.

[3] D. F. Geesaman, K. Saito, and A. W. Thomas, "The nuclear EMC effect," *Ann. Rev. Nucl. Part. Sci.*, vol. 45, pp. 337–390, 1995.

[4] P. R. Norton, "The EMC effect," *Rept. Prog. Phys.*, vol. 66, pp. 1253–1297, 2003.

[5] O. Hen, D. W. Higinbotham, G. A. Miller, E. Piasetzky, and L. B. Weinstein, "The EMC Effect and High Momentum Nucleons in Nuclei," *Int. J. Mod. Phys. E*, vol. 22, p. 1330017, 2013.

[6] O. Hen, G. A. Miller, E. Piasetzky, and L. B. Weinstein, "Nucleon-Nucleon Correlations, Short-lived Excitations, and the Quarks Within," *To appear in 'Reviews of Modern Physics', arXiv:nucl-ex/1611.09748*, 2016.

[7] J. Arrington, D. W. Higinbotham, G. Rosner, and M. Sargsian, "Hard probes of short-range nucleon-nucleon correlations," *Prog. Part. Nucl. Phys.*, vol. 67, pp. 898–938, 2012.

[8] L. L. Frankfurt and M. I. Strikman, "Hard Nuclear Processes and Microscopic Nuclear Structure," *Phys. Rept.*, vol. 160, pp. 235–427, 1988.

[9] A. B. Larionov and M. Strikman, "Exploring QCD dynamics in medium energy γA semiexclusive collisions," *Phys. Lett. B*, vol. 760, pp. 753–758, 2016.

[10] B. Clasie *et al.*, "Measurement of Nuclear Transparency for the $A(e, e^{'}\pi^{+})$ Reaction," *Phys. Rev. Lett.*, vol. 99, p. 242502, 2007.

[11] L. El Fassi *et al.*, "Evidence for the onset of color transparency in ρ^0 electroproduction off nuclei," *Phys. Lett. B*, vol. 712, pp. 326–330, 2012.

[12] J. Aclander *et al.*, "Nuclear transparency in $90^{\circ}_{\rm c.m.}$ quasielastic $A(p, 2p)$ reactions," *Phys. Rev. C*, vol. 70, p. 015208, 2004.

[13] K. Garrow *et al.*, "Nuclear transparency from quasielastic $A(e, e^{'}p)$ reactions up to $Q^2 = 8.1({\rm GeV}/c)^2$," *Phys. Rev. C*, vol. 66, p. 044613, 2002.

[14] M. Strikman, "QCD factorization theorems for DIS exclusive processes and inclusive diffraction: New probes of hadrons and nuclei," *Nucl. Phys. A*, vol. 663, pp. 64–73, 2000.

[15] R. J. Glauber, *Lectures in theoretical physics*, vol. 1. Interscience Publ., 1959.

[16] M. R. Frank, B. K. Jennings, and G. A. Miller, "The Role of color neutrality in nuclear physics: Modifications of nucleonic wave functions," *Phys. Rev. C*, vol. 54, pp. 920–935, 1996.

[17] L. L. Frankfurt and M. I. Strikman, "Point-like Configurations in Hadrons and Nuclei and Deep Inelastic Reactions with Leptons: EMC and EMC-like Effects," *Nucl. Phys. B*, vol. 250, pp. 143–176, 1985.

[18] S. J. Brodsky and G. R. Farrar, "Scaling Laws at Large Transverse Momentum," *Phys. Rev. Lett.*, vol. 31, pp. 1153–1156, 1973.

[19] S. J. Brodsky and G. R. Farrar, "Scaling Laws for Large Momentum Transfer Processes," *Phys. Rev. D*, vol. 11, p. 1309, 1975.

[20] V. A. Matveev, R. M. Muradian, and A. N. Tavkhelidze, "Automodellism in the large - angle elastic scattering and structure of hadrons," *Lett. Nuovo Cim.*, vol. 7, pp. 719–723, 1973.

[21] B.-J. Cai and B.-A. Li, "Effects of short-range correlations on nuclear symmetry energy within a modified Gogny-Hartree-Fock energy density functional approach," *arXiv:nucl-th/1703.08743*, 2017.

[22] O. Hen, B.-A. Li, W.-J. Guo, L. B. Weinstein, and E. Piasetzky, "Symmetry Energy of Nucleonic Matter With Tensor Correlations," *Phys. Rev. C*, vol. 91, no. 2, p. 025803, 2015.

[23] L. B. Weinstein, E. Piasetzky, D. W. Higinbotham, J. Gomez, O. Hen, and R. Shneor, "Short Range Correlations and the EMC Effect," *Phys. Rev. Lett.*, vol. 106, p. 052301, 2011.

[24] O. Hen *et al.*, "Momentum sharing in imbalanced Fermi systems," *Science*, vol. 346, pp. 614–617, 2014.

[25] M. M. Sargsian, "New properties of the high-momentum distribution of nucleons in asymmetric nuclei," *Phys. Rev. C*, vol. 89, no. 3, p. 034305, 2014.

[26] R. Subedi *et al.*, "Probing Cold Dense Nuclear Matter," *Science*, vol. 320, pp. 1476–1478, 2008.

[27] I. Korover *et al.*, "Probing the Repulsive Core of the Nucleon-Nucleon Interaction via the $^4He(e, epN)$ Triple-Coincidence Reaction," *Phys. Rev. Lett.*, vol. 113, no. 2, p. 022501, 2014.

[28] A. Tang *et al.*, "*n-p* short range correlations from $(p, 2p + n)$ measurements," *Phys. Rev. Lett.*, vol. 90, p. 042301, 2003.

[29] E. Piasetzky, M. Sargsian, L. Frankfurt, M. Strikman, and J. W. Watson, "Evidence for the strong dominance of proton-neutron correlations in nuclei," *Phys. Rev. Lett.*, vol. 97, p. 162504, 2006.

[30] R. Shneor *et al.*, "Investigation of proton-proton short-range correlations via the $^{12}\mathrm{C}(e, e'pp)$ reaction," *Phys. Rev. Lett.*, vol. 99, p. 072501, 2007.

[31] E. M. Aitala *et al.*, "Direct measurement of the pion valence quark momentum distribution, the pion light cone wave function squared," *Phys. Rev. Lett.*, vol. 86, pp. 4768–4772, 2001.

[32] L. Frankfurt, G. A. Miller, and M. Strikman, "Coherent nuclear diffractive production of mini - jets: Illuminating color transparency," *Phys. Lett. B*, vol. 304, pp. 1–7, 1993.

[33] G. R. Farrar, H. Liu, L. L. Frankfurt, and M. I. Strikman, "Transparency in Nuclear Quasiexclusive Processes with Large Momentum Transfer," *Phys. Rev. Lett.*, vol. 61, pp. 686–689, 1988.

[34] B. K. Jennings and G. A. Miller, "On Color Transparency," *Phys. Lett. B*, vol. 236, pp. 209–213, 1990.

[35] B. K. Jennings and G. A. Miller, "Color transparency: The Wherefore and the why," *Phys. Rev. D*, vol. 44, pp. 692–703, 1991.

[36] B. K. Jennings and G. A. Miller, "Realistic hadronic matrix element approach to color transparency," *Phys. Rev. Lett.*, vol. 69, pp. 3619–3622, 1992.

[37] A. S. Carroll *et al.*, "Nuclear Transparency to Large Angle *pp* Elastic Scattering," *Phys. Rev. Lett.*, vol. 61, pp. 1698–1701, 1988.

[38] I. Mardor *et al.*, "Nuclear transparency in large momentum transfer quasielastic scattering," *Phys. Rev. Lett.*, vol. 81, pp. 5085–5088, 1998.

[39] A. Leksanov *et al.*, "Energy dependence of nuclear transparency in C$(p, 2p)$ scattering," *Phys. Rev. Lett.*, vol. 87, p. 212301, 2001.

[40] N. Makins *et al.*, "Momentum transfer dependence of nuclear transparency from the quasielastic ^{12}C(e,e'p) reaction," *Phys. Rev. Lett.*, vol. 72, pp. 1986–1989, 1994.

[41] T. G. O'Neill *et al.*, "A-dependence of nuclear transparency in quasielastic $A(e, e'p)$ at high Q^2," *Phys. Lett. B*, vol. 351, pp. 87–92, 1995.

[42] D. Abbott *et al.*, "Quasifree $(e, e'p)$ reactions and proton propagation in nuclei," *Phys. Rev. Lett.*, vol. 80, pp. 5072–5076, 1998.

[43] S. Frullani and J. Mougey, "Single-particle properties of nuclei through $(e, e'p)$ reactions," *Advances in Nuclear Physics*, vol. 14, 1984.

[44] D. Dutta *et al.*, "Jefferson Lab 12 GeV experiment E12-06-107." https://misportal.jlab.org/mis/physics/experiments/viewProposal.cfm?paperId=686.

[45] B. Blaettel, G. Baym, L. L. Frankfurt, and M. Strikman, "How transparent are hadrons to pions?," *Phys. Rev. Lett.*, vol. 70, pp. 896–899, 1993.

[46] A. Larson, G. A. Miller, and M. Strikman, "Pionic Color Transparency," *Phys. Rev. C*, vol. 74, p. 018201, 2006.

[47] W. Cosyn, M. C. Martinez, J. Ryckebusch, and B. Van Overmeire, "Nuclear transparencies from photoinduced pion production," *Phys. Rev. C*, vol. 74, p. 062201, 2006.

[48] M. M. Kaskulov, K. Gallmeister, and U. Mosel, "Pionic transparency in semi-exclusive electroproduction off nuclei," *Phys. Rev. C*, vol. 79, p. 015207, 2009.

[49] L. Frankfurt, G. A. Miller, and M. Strikman, "Color Transparency in Semi-Inclusive Electroproduction of rho Mesons," *Phys. Rev. C*, vol. 78, p. 015208, 2008.

[50] K. Gallmeister, M. Kaskulov, and U. Mosel, "Color transparency in hadronic attenuation of ρ^0 mesons," *Phys. Rev. C*, vol. 83, p. 015201, 2011.

[51] K. Hafidi *et al.*, "Jefferson Lab 12 GeV experiment E12-06-106." https://misportal.jlab.org/mis/physics/experiments/viewProposal.cfm?paperId=685.

[52] D. Dutta *et al.*, "Nuclear transparency with the $\gamma n \to \pi^- p$ process in ^{4}He," *Phys. Rev. C*, vol. 68, p. 021001, 2003.

[53] M. Alvioli, C. Ciofi degli Atti, and H. Morita, "Proton-neutron and proton-proton correlations in medium-weight nuclei and the role of the tensor force," *Phys. Rev. Lett.*, vol. 100, p. 162503, 2008.

[54] R. Schiavilla, R. B. Wiringa, S. C. Pieper, and J. Carlson, "Tensor Forces and the Ground-State Structure of Nuclei," *Phys. Rev. Lett.*, vol. 98, p. 132501, 2007.

[55] M. M. Sargsian, T. V. Abrahamyan, M. I. Strikman, and L. L. Frankfurt, "Exclusive electrodisintegration of ^{3}He at high Q2. II. Decay function formalism," *Phys. Rev. C*, vol. 71, p. 044615, 2005.

[56] R. B. Wiringa, R. Schiavilla, S. C. Pieper, and J. Carlson, "Nucleon and nucleon-pair momentum distributions in $A \leq 12$ nuclei," *Phys. Rev. C*, vol. 89, no. 2, p. 024305, 2014.

[57] C. Ciofi degli Atti and S. Simula, "Realistic model of the nucleon spectral function in few and many nucleon systems," *Phys. Rev. C*, vol. 53, p. 1689, 1996.

[58] C. Colle, W. Cosyn, J. Ryckebusch, and M. Vanhalst, "Factorization of exclusive electron-induced two-nucleon knockout," *Phys. Rev. C*, vol. 89, no. 2, p. 024603, 2014.

[59] R. L. Anderson, D. Gustavson, D. Ritson, G. A. Weitsch, H. J. Halpern, R. Prepost, D. H. Tompkins, and D. E. Wiser, "Measurements of exclusive photoproduction processes at large values of t and u from 4 to 7.5 GeV," *Phys. Rev. D*, vol. 14, p. 679, 1976.

[60] Arrington, J. and others, "Jefferson Lab 12 GeV experiment E12-11-112." http://hallaweb.jlab.org/collab/PAC/PAC38/Tritium-isospin.pdf.

[61] O. Hen, L. B. Weinstein, S. Gilad, and W. Boeglin, "Proton and Neutron Momentum Distributions in $A = 3$ Asymmetric Nuclei," *arXiv/nucl-ex:1410:4451*, 2014.

[62] Hen, O. and others, "Jefferson Lab 12 GeV experiment E12-11-003A." https://www.jlab.org/exp_prog/proposals/15/E12-11-003A.pdf.

[63] O. Hen, L. B. Weinstein, S. Gilad, and S. A. Wood, "In Medium Nucleon Structure Functions, SRC, and the EMC effect," *arXiv/nucl-ex:1409.1717*, 2014.

A Integrated cross section

To validate our simulation, we performed a back-of-the-envelope calculation of the rate of the $\gamma+n \to \pi^- + p$ reaction. The differential cross section for the reaction can be approximated using the following:

$$\frac{d\sigma}{dt} = C \cdot f(s) \cdot f(\cos\theta_{cm}) \approx 1.25 \cdot 10^7 \text{nb} \cdot \text{GeV}^{12} \cdot s^{-7} \cdot (1-\cos\theta_{cm})^{-5}(1+\cos\theta_{cm})^{-4}, \quad (1)$$

where the cross section is in units of nb/GeV^2, and θ_{cm} is the polar scattering angle in the center of mass system.

The polar scattering angle in the center of mass system θ_{cm} can be approximated as

$$\cos\theta_{cm} = \frac{t - m_\pi^2 + 2k_i\sqrt{k_f^2 + m_\pi^2}}{2k_i k_f}, \quad (2)$$

where k_i, and k_f are the center of mass momenta of incoming and outgoing particles:

$$k_i = \frac{s - m_p^2}{2\sqrt{s}} \quad (3)$$

$$k_f = \sqrt{\frac{(s-(m_p-m_\pi)^2)\cdot(s-(m_p+m_\pi)^2)}{4s}}. \quad (4)$$

Equation (2) shows that for $\theta_{cm} > 41^\circ$, $|t| > 2$ (GeV/c)^2. Mandelstam variables are interrelated as $s+t+u = m^2$, which means that for $E_\gamma = 9$ GeV we have $|t| > 2$ (GeV/c)^2 and $|u| > 2$ (GeV/c)^2 for almost the whole range of θ_{cm} between 40° and 140°.

The cross section (1) in terms of $\cos\theta_{cm}$:

$$d\sigma = C \cdot s^{-7} \cdot f(\cos\theta_{cm})dt = C_1 \cdot s^{-7} \cdot f(\cos\theta_{cm})d\cos\theta_{cm}, \quad (5)$$

where $C_1 = 1.25 \cdot 10^7 \cdot 2k_i k_f$.

The total cross section for $E_\gamma = 9$ GeV and θ_{cm} in the range between 40° and 140° is then about 2.1 nb. The number of expected MF events per day on a carbon target is

$$N = \sigma_{nucl} \cdot F \cdot T \cdot t \cdot \epsilon = 880, \quad (6)$$

where $F = 2 \cdot 10^7$ photons/s - photon flux on target, $T = 1.45 \cdot 10^{23}$ atoms/cm^2 - target density for ^{12}C, $t = 24$ hours $\cdot 3600$ s/hour - time, $\epsilon = 0.64$ - detection efficiency, and $\sigma_{nucl} = \sigma \cdot A/2 \cdot A^{-1/3} = 5.5$ nb - nuclear cross section for ^{12}C. This is consistent within 20% with the simulation results (740 events/day for the ^{12}C target).